angular momentum. (c) To examine whether there might be an explanation for this effect in terms of the 0^+ and 2^+ nuclear wave functions, make a similar tabulation of decays from 1^- states, that is, of $1^- \rightarrow 0^+$ and $1^- \rightarrow 2^+$ decays. Both these first-forbidden decays carry one unit of total angular momentum. (Why?) Do you observe a systematic difference in *ft* values between 0^+ and 2^+ final states? What do you conclude about the probable effect of the final nuclear state on the β decays from 2^- initial states?

26. There are several examples of allowed β decays that have larger than average *ft* values, which can be explained with reference to the nuclear structure. Consider, for example, the following cases: (a) $^{65}\text{Ni} \rightarrow {}^{65}\text{Cu}$ and $^{65}\text{Zn} \rightarrow {}^{65}\text{Cu}$, in which the ground state-ground state decays are both $\frac{5}{2}^-$ to $\frac{3}{2}^-$ Gamow-Teller decays, but the *ft* values are 1–2 orders of magnitude larger than for allowed decays to other low-lying states; (b) $^{115}\text{Te} \rightarrow {}^{115}\text{Sb}$ and $^{115}\text{Sb} \rightarrow {}^{115}\text{Sn}^*$; in the ^{115}Te decay, the $\frac{7}{2}^+ \rightarrow \frac{5}{2}^+$ transition to the ^{115}Sb ground state is not seen, and in the ^{115}Sb decay, a $\frac{7}{2}^+$ low-lying excited state is populated only weakly, with an *ft* value again 1–2 orders of magnitude larger than values for neighboring excited states. Find the shell model identification of these states and thus explain why the allowed decay mode is inhibited. Use the *Table of Isotopes* to find other examples of inhibited decays with the same shell-model assignments.

10 GAMMA DECAY

Most α and β decays, and in fact most nuclear reactions as well, leave the final nucleus in an excited state. These excited states decay rapidly to the ground state through the emission of one or more γ rays, which are photons of electromagnetic radiation like X rays or visible light. Gamma rays have energies typically in the range of 0.1 to 10 MeV, characteristic of the energy difference between nuclear states, and thus corresponding wavelengths between 10^4 and 100 fm. These wavelengths are far shorter than those of the other types of electromagnetic radiations that we normally encounter; visible light, for example, has wavelengths 10^6 times longer than γ rays.

The detail and richness of our knowledge of nuclear spectroscopy depends on what we know of the excited states, and so studies of γ-ray emission have become the standard technique of nuclear spectroscopy. Other factors that contribute to the popularity and utility of this method include the relative ease of observing γ rays (negligible absorption and scattering in air, for instance, contrary to the behavior of α and β radiations) and the accuracy with which their energies (and thus by deduction the energies of the excited states) can be measured. Furthermore, studying γ emission and its competing process, internal conversion, allows us to deduce the spins and parities of the excited states.

10.1 ENERGETICS OF γ DECAY

Let's consider the decay of a nucleus of mass M at rest, from an initial excited state E_i to a final state E_f. To conserve linear momentum, the final nucleus will not be at rest but must have a recoil momentum p_R and corresponding recoil kinetic energy T_R, which we assume to be nonrelativistic ($T_R = p_R^2/2M$). Conservation of total energy and momentum give

$$\begin{aligned} E_i &= E_f + E_\gamma + T_R \\ 0 &= \boldsymbol{p}_R + \boldsymbol{p}_\gamma \end{aligned} \tag{10.1}$$

It follows that $p_R = p_\gamma$; the nucleus recoils with a momentum equal and opposite to that of the γ ray. Defining $\Delta E = E_i - E_f$ and using the relativistic relationship $E_\gamma = cp_\gamma$,

$$\Delta E = E_\gamma + \frac{E_\gamma^2}{2Mc^2} \tag{10.2}$$

which has the solution

$$E_\gamma = Mc^2\left[-1 \pm \left(1 + 2\frac{\Delta E}{Mc^2}\right)^{1/2}\right] \tag{10.3}$$

The energy differences ΔE are typically of the order of MeV, while the rest energies Mc^2 are of order $A \times 10^3$ MeV, where A is the mass number. Thus $\Delta E \ll Mc^2$ and to a precision of the order of 10^{-4} to 10^{-5} we keep only the first three terms in the expansion of the square root:

$$E_\gamma \cong \Delta E - \frac{(\Delta E)^2}{2Mc^2} \tag{10.4}$$

which also follows directly from Equation 10.2 with the approximation $\Delta E \cong E_\gamma$.

The actual γ-ray energy is thus diminished somewhat from the maximum available decay energy ΔE. This recoil correction to the energy is generally negligible, amounting to a 10^{-5} correction that is usually far smaller than the experimental uncertainty with which we can measure energies. There is one circumstance in which the recoil plays an important role; this case, known as the Mössbauer effect, is discussed in Section 10.9. Except for this case, we will in the remainder of this chapter assume $E_\gamma = \Delta E$.

For low-energy γ rays, the recoil energy is less than 1 eV and has a negligible effect. High-energy γ rays (such as the 5–10-MeV radiations emitted following neutron capture) give recoils in the range of 100 eV, which may be sufficient to drive the recoiling atom from its position in a solid lattice. Effects of this sort are known as *radiation damage* and have an important place in the study of solids.

10.2 CLASSICAL ELECTROMAGNETIC RADIATION

As you will recall from your study of modern physics, electromagnetic radiation can be treated either as a classical wave phenomenon or else as a quantum phenomenon. The type of treatment we use is determined by the kind of physical effect we are trying to describe. For analyzing radiations from individual atoms and nuclei the quantum description is most appropriate, but we can more easily understand the quantum calculations of electromagnetic radiation if we first review the classical description.

Static (i.e., constant in time) distributions of charges and currents give static electric and magnetic fields. In Section 3.5, we discussed how these fields can be analyzed in terms of the *multipole moments* of the charge distribution—dipole moment, quadrupole moment, and so on. These multipole moments give characteristic fields, and we can conveniently study the dipole field, quadrupole field, and so on.

If the charge and current distributions vary with time, particularly if they vary sinusoidally with circular frequency ω, a *radiation field* is produced. The radiation field (which is studied at a distance from the source that is large compared with the size of the source) can be analyzed, like the static field, in terms of its multipole character. As an example, we consider the lowest multipole order, the dipole field.

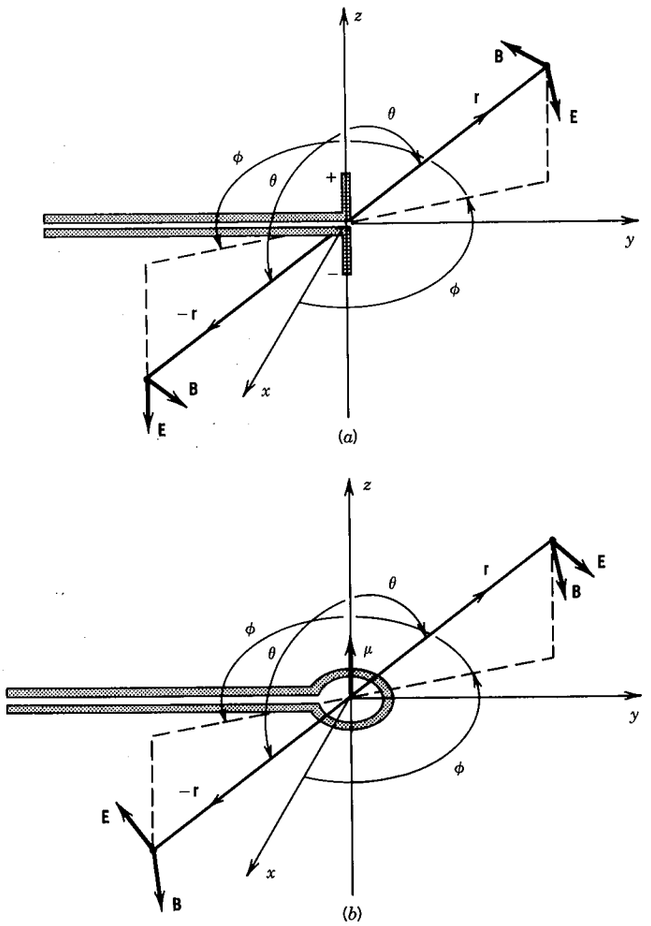

Figure 10.1 Electric and magnetic fields from (*a*) an electric dipole and (*b*) a magnetic dipole. In each case the dipole moment is along the z axis. The vectors show the radiation fields $\boldsymbol{E}$ and $\boldsymbol{B}$ at a particular instant of time. The wires along the negative y axes should be imagined as connected to a current source of frequency ω, and to be twisted so as to make no contribution themselves to the radiation. Also shown are the behaviors of $\boldsymbol{E}$ and $\boldsymbol{B}$ under the spatial reflection $\boldsymbol{r} \rightarrow -\boldsymbol{r}$; note the differences between the two cases.

A static *electric* dipole consists of equal and opposite charges $+q$ and $-q$ separated by a fixed distance z; the electric dipole moment is then $d = qz$. A static *magnetic* dipole can be represented as a circular current loop of current i enclosing area A; the magnetic dipole moment is $\mu = iA$. We can produce electromagnetic radiation fields by varying the dipole moments; for example, we can allow the charges to oscillate along the z axis, so that $d(t) = qz\cos\omega t$, thereby producing an electric dipole radiation field. Similarly, we could vary the current so that $\mu(t) = iA\cos\omega t$. Figure 10.1 shows the radiation fields produced in these two cases. The alternating electric dipole, Figure 10.1*a*, can be regarded

as a linear current element, for which the magnetic field lines form circles concentric with the z axis. The magnetic field vector $\boldsymbol{B}$ is tangent to the circles, and the electric field direction must be chosen so that $\boldsymbol{E} \times \boldsymbol{B}$ is in the direction of propagation of the radiation. The magnetic dipole, Figure 10.1*b*, has the magnetic field lines that we often associate with a bar magnet.

There are three characteristics of the dipole radiation field that are important for us to consider:

1. The power radiated into a small element of area, in a direction at an angle θ with respect to the z axis, varies as $\sin^2\theta$. The average radiated power can be calculated based on wave theory or on quantum theory, and by the correspondence principle the two calculations must agree when we extend the quantum result to the classical limit. This characteristic $\sin^2\theta$ dependence of dipole radiation must therefore be a characteristic result of the quantum calculation as well. Higher order multipoles, such as quadrupole radiation, have a different angular distribution. In fact, as we shall see, measuring the angular distribution of the radiation is a convenient way to determine which multipoles are present in the radiation.
2. Electric and magnetic dipole fields have opposite parity. Consider the effect of the transformation $\boldsymbol{r} \rightarrow -\boldsymbol{r}$. The magnetic field of the electric dipole clearly changes sign; thus $\boldsymbol{B}(\boldsymbol{r}) = -\boldsymbol{B}(-\boldsymbol{r})$. For the magnetic dipole, on the other hand, there is no change of sign, so $\boldsymbol{B}(\boldsymbol{r}) = \boldsymbol{B}(-\boldsymbol{r})$. Thus the electric and magnetic dipoles, which give identical angular distributions, differ in the parity of the radiation fields. Electric dipole radiation has odd parity, while magnetic dipole radiation has even parity.
3. The average radiated power (energy emitted per unit time) is

$$P = \frac{1}{12\pi\epsilon_0}\frac{\omega^4}{c^3}d^2 \tag{10.5}$$

for electric dipoles, and

$$P = \frac{1}{12\pi\epsilon_0}\frac{\omega^4}{c^5}\mu^2 \tag{10.6}$$

for magnetic dipoles. Here d and μ represent the *amplitudes* of the time-varying dipole moments.

Without entering into a detailed discussion of electromagnetic theory, we can extend these properties of dipole radiation to multipole radiation in general. We first define the index L of the radiation so that 2^L is the multipole order ($L = 1$ for dipole, $L = 2$ for quadrupole, and so on). With E for electric and M for magnetic, we can generalize the above three properties of dipole radiation.

1. The angular distribution of 2^L-pole radiation, relative to a properly chosen direction, is governed by the *Legendre polynomial* $P_{2L}(\cos\theta)$. The most common cases are dipole, for which $P_2 = \frac{1}{2}(3\cos^2\theta - 1)$, and quadrupole, with $P_4 = \frac{1}{8}(35\cos^4\theta - 30\cos^2\theta + 3)$.

2. The parity of the radiation field is

$$\pi(ML) = (-1)^{L+1}$$
$$\pi(EL) = (-1)^{L} \tag{10.7}$$

Notice that electric and magnetic multipoles of the same order always have opposite parity.

3. The radiated power is, using $\sigma = E$ or M to represent electric or magnetic radiation,

$$P(\sigma L) = \frac{2(L+1)c}{\epsilon_0 L[(2L+1)!!]^2}\left(\frac{\omega}{c}\right)^{2L+2}[m(\sigma L)]^2 \tag{10.8}$$

where $m(\sigma L)$ is the amplitude of the (time-varying) electric or magnetic multipole moment, and where the double factorial $(2L+1)!!$ indicates $(2L+1)\cdot(2L-1)\cdots 3\cdot 1$. The generalized multipole moment $m(\sigma L)$ differs, for $L = 1$, from the electric dipole moment d and magnetic dipole moment μ through some relatively unimportant numerical factors of order unity. From now on, we shall deal only with the generalized moments in our discussion of γ radiation.

10.3 TRANSITION TO QUANTUM MECHANICS

To carry the classical theory into the quantum domain, all we must do is quantize the sources of the radiation field, the classical multipole moments. In Equation 10.8, it is necessary to replace the *multipole moments* by appropriate *multipole operators* that change the nucleus from its initial state ψ_i to the final state ψ_f. As we have discussed for α and β radiation, the decay probability is governed by the *matrix element* of the *multipole operator*

$$m_{fi}(\sigma L) = \int \psi_f^* m(\sigma L)\psi_i \, dv \tag{10.9}$$

The integral is carried out over the volume of the nucleus. We shall not discuss the form of the operator $m(\sigma L)$, except to say that its function is to change the nuclear state from ψ_i to ψ_f while simultaneously creating a photon of the proper energy, parity, and multipole order.

If we regard Equation 10.8 as the energy radiated per unit time in the form of photons, each of which has energy $\hbar\omega$, then the probability per unit time for photon emission (that is, the decay constant) is

$$\lambda(\sigma L) = \frac{P(\sigma L)}{\hbar\omega} = \frac{2(L+1)}{\epsilon_0\hbar L[(2L+1)!!]^2}\left(\frac{\omega}{c}\right)^{2L+1}[m_{fi}(\sigma L)]^2 \tag{10.10}$$

This expression for the decay constant can be carried no further until we evaluate the matrix element $m_{fi}(\sigma L)$, which requires knowledge of the initial and final wave functions. We can simplify the calculation and make some corresponding estimates of the γ-ray emission probabilities if we assume the transition is due to a single proton that changes from one shell-model state to another. In the case of electric transitions, the multipole operator includes a term of the form $er^L Y_{LM}(\theta, \phi)$, which reduces to ez for $L = 1$ (dipole) radiation as expected, and to $e(3z^2 - r^2)$ for $L = 2$ (quadrupole) radiation, analogous to the calculation of

the static quadrupole moment in Equation 3.36. If we take the radial parts of the nuclear wave functions ψ_i and ψ_f to be constant up to the nuclear radius R and zero for $r > R$, then the radial part of the transition probability is of the form

$$\int_0^R r^2 r^L dr \Big/ \int_0^R r^2 dr = \frac{3}{L+3} R^L \tag{10.11}$$

where the integral in the denominator is included for normalization and the r^2 factor comes from the volume element. Including this factor in the matrix element, and replacing the angular integrals by unity, which is also a reasonable estimate, the EL transition probability is estimated to be

$$\lambda(EL) \cong \frac{8\pi(L+1)}{L[(2L+1)!!]^2} \frac{e^2}{4\pi\epsilon_0 \hbar c} \left(\frac{E}{\hbar c}\right)^{2L+1} \left(\frac{3}{L+3}\right)^2 cR^{2L} \tag{10.12}$$

With $R = R_0 A^{1/3}$, we can make the following estimates for some of the lower multipole orders

$$\begin{aligned} \lambda(E1) &= 1.0 \times 10^{14} A^{2/3} E^3 \\ \lambda(E2) &= 7.3 \times 10^{7} A^{4/3} E^5 \\ \lambda(E3) &= 34 A^2 E^7 \\ \lambda(E4) &= 1.1 \times 10^{-5} A^{8/3} E^9 \end{aligned} \tag{10.13}$$

where λ is in s^{-1} and E is in MeV.

For magnetic transitions, the radial integral includes the term r^{L-1}, and the same assumption as above about the constancy of the nuclear wave function gives the factor $3R^{L-1}/(L+2)$. The magnetic operator also includes a factor that depends on the nuclear magnetic moment of the proton. The result for the ML transition probability is

$$\lambda(ML) \cong \frac{8\pi(L+1)}{L[(2L+1)!!]^2} \left(\mu_p - \frac{1}{L+1}\right)^2 \left(\frac{\hbar}{m_p c}\right)^2 \left(\frac{e^2}{4\pi\epsilon_0 \hbar c}\right) \times \left(\frac{E}{\hbar c}\right)^{2L+1} \left(\frac{3}{L+2}\right)^2 cR^{2L-2} \tag{10.14}$$

where again several angular momentum factors of order unity have been neglected. It is customary to replace the factor $[\mu_p - 1/(L+1)]^2$ by 10, which gives the following estimates for the lower multiple orders*:

$$\begin{aligned} \lambda(M1) &= 5.6 \times 10^{13} E^3 \\ \lambda(M2) &= 3.5 \times 10^{7} A^{2/3} E^5 \\ \lambda(M3) &= 16 A^{4/3} E^7 \\ \lambda(M4) &= 4.5 \times 10^{-6} A^2 E^9 \end{aligned} \tag{10.15}$$

*The numerical coefficients in Equation 10.15 differ slightly from those sometimes found in the literature. The difference arises because the factor $3/(L+2)$ in Equation 10.14 is often replaced by $3/(L+3)$, to make Equation 10.14 look more like Equation 10.12. We choose to maintain the form of Equation 10.14, so that to agree with some ML Weisskopf estimates in the literature, Equations 10.15 must be multiplied by $(L+2)^2/(L+3)^2$.

These estimates for the transition rates are known as *Weisskopf estimates* and are not meant to be true theoretical calculations to be compared with measured transition rates. Instead, they provide us with reasonable relative comparisons of the transition rates. For example, if the observed decay rate of a certain γ transition is many orders of magnitude smaller than the Weisskopf estimate, we might suspect that a poor match-up of initial and final wave functions is slowing the transition. Similarly, if the transition rate were much greater than the Weisskopf estimate, we might guess that more than one single nucleon is responsible for the transition.

Based on the Weisskopf estimates, we can immediately draw two conclusions about transition probabilities: (1) The lower multipolarities are dominant—increasing the multipole order by one unit reduces the transition probability by a factor of about 10^{-5}. A similar effect occurs in atoms, in which the most common transitions are dipole. (2) For a given multipole order, electric radiation is more likely than magnetic radiation by about two orders of magnitude in medium and heavy nuclei. We shall see in Section 10.7 how these expectations agree with observations.

10.4 ANGULAR MOMENTUM AND PARITY SELECTION RULES

A classical electromagnetic field produced by oscillating charges and currents transmits not only energy but angular momentum as well. If, for example, we surround the charges and currents with a large spherical absorbing shell, the shell can be made to rotate by the absorbed radiation. The rate at which angular momentum is radiated is proportional to the rate at which energy is radiated.

When we go over to the quantum limit, we can preserve the proportionality if each photon carries a definite angular momentum. The multipole operator of order L includes the factor $Y_{LM}(\theta, \phi)$, which is associated with an angular momentum L. We therefore conclude that a multipole of order L transfers an angular momentum of $L\hbar$ per photon.

Let's consider a γ transition from an initial excited state of angular momentum I_i and parity π_i to a final state I_f and π_f. For the moment we will assume $I_i \neq I_f$. Conservation of angular momentum requires that the total initial angular momentum be equal to the total final angular momentum. In vector terms,

$$\boldsymbol{I}_i = \boldsymbol{L} + \boldsymbol{I}_f$$

Since $\boldsymbol{I}_i$, $\boldsymbol{L}$, and $\boldsymbol{I}_f$ must form a closed vector triangle, the possible values of L are restricted. The largest possible value of L is $I_i + I_f$ and the smallest possible value is $|I_i - I_f|$. For example, if $I_i = \frac{3}{2}$ and $I_f = \frac{5}{2}$, the possible values of L are 1, 2, 3, and 4; the radiation field in this case would consist of a mixture of dipole, quadrupole, octupole ($L = 3$) and hexadecapole ($L = 4$) radiation.

Whether the emitted radiation is of the electric or magnetic type is determined by the relative parity of the initial and final levels. If there is no change in parity ($\Delta\pi$ = no), then the radiation field must have even parity; if the parity changes in the transition ($\Delta\pi$ = yes), then the radiation field must have odd parity. As shown by Equation 10.7, electric and magnetic multipoles differ in their parities. Electric transitions have even parity if L = even, while magnetic transitions have

even parity if L = odd. Therefore a $\Delta\pi$ = no transition would consist of even electric multipoles and odd magnetic multipoles. A $\Delta\pi$ = yes transition, on the other hand, would consist of odd electric and even magnetic multipoles. In our previous example ($I_i = \frac{3}{2}$ to $I_f = \frac{5}{2}$), let us assume that $\pi_i = \pi_f$, so that $\Delta\pi$ = no. We have already concluded that $L = 1, 2, 3$, or 4. The $L = 1$ radiation must be of magnetic character (odd magnetic and even electric multipoles for $\Delta\pi$ = no), the $L = 2$ radiation of electric character, and so on. The radiation field must thus be $M1$, $E2$, $M3$, and $E4$ radiation. If our two states had $\pi_i = -\pi_f$ ($\Delta\pi$ = yes) then the radiation field would be $E1$, $M2$, $E3$, and $M4$ radiation.

We therefore have the following angular momentum and parity *selection rules*:

$$\begin{aligned} &|I_i - I_f| \le L \le I_i + I_f \qquad (\text{no } L = 0) \\ &\Delta\pi = \text{no:} \qquad \text{even electric, odd magnetic} \\ &\Delta\pi = \text{yes:} \qquad \text{odd electric, even magnetic} \end{aligned} \tag{10.16}$$

The exception to the angular momentum selection rule occurs when $I_i = I_f$ because *there are no monopole* ($L = 0$) *transitions* in which a single photon is emitted. Classically, the monopole moment is just the electric charge, which does not vary with time. (A spherical charge distribution of radius R gives only a pure $1/r^2$ Coulomb field for $r > R$. Even if we allow the sphere to undergo radial oscillations, the Coulomb field for $r > R$ is unaffected and no radiation is produced.) For transitions in which $I_i = I_f$, the lowest possible γ-ray multipole order is dipole ($L = 1$).

The case in which either I_i or I_f is zero is particularly simple, for then only a pure multipole transition is emitted. For example, the first excited 2^+ ($I_i = 2$, π_i = even) state in even-Z, even-N nuclei decays to the 0^+ ground state through the emission of a pure electric quadrupole ($E2$) transition. The above selection rules give immediately $L = 2$ and electric radiation for $\Delta\pi$ = no.

For $I_i = I_f = 0$, the selection rules would give only $L = 0$, which as we have already discussed is not permitted for radiative transitions. A few even-even nuclei have 0^+ first excited states, which are forbidden to decay to the 0^+ ground state by γ emission. These states decay instead through *internal conversion*, which we discuss in Section 10.6. In this process the excitation energy is emitted by ejecting an *orbital* electron, the wave function of which penetrates the nuclear volume and samples the monopole distribution at $r < R$, where the potential *does* fluctuate.

Usually the spins I_i and I_f have values for which the selection rules permit several multipoles to be emitted. The single-particle (Weisskopf) estimates permit us to make some general predictions about which multipole is most likely to be emitted. Let us consider the previous example of an $I_i = \frac{3}{2}^+$ to $I_f = \frac{5}{2}^+$ transition ($M1$, $E2$, $M3$, $E4$). We assume a medium-weight nucleus ($A = 125$, so $A^{2/3} = 25$) and a transition energy $E = 1$ MeV. The estimates (Equations 10.13 and 10.15) give emission probabilities in the ratio

$$\lambda(M1) : \lambda(E2) : \lambda(M3) : \lambda(E4) = 1 : 1.4 \times 10^{-3} : 2.1 \times 10^{-10} : 1.3 \times 10^{-13}$$

You can see that the lower multipoles ($M1$ and $E2$) are far more likely than the higher ones. In practice we could regard this transition as being composed of $M1$ radiation with possibly a small mixture of $E2$. If the transition were $\Delta\pi$ = yes, the multipoles would be $E1$, $M2$, $E3$, $M4$ with the ratios

$$\lambda(E1) : \lambda(M2) : \lambda(E3) : \lambda(M4) = 1 : 2.3 \times 10^{-7} : 2.1 \times 10^{-10} : 2.1 \times 10^{-17}$$

Here only the $E1$ is expected to contribute to the transition.

There are rather general expectations, based on the single-particle estimates:

1. The lowest permitted multipole usually dominates.
2. Electric multipole emission is more probable than the same magnetic multipole emission by a factor of order 10^2 for medium and heavy nuclei. (Of course, the selection rules prohibit EL and ML from competing in the same radiation field.)
3. Emission of multipole $L + 1$ is less probable than emission of multipole L by a factor of the order of about 10^{-5}.
4. Combining 2 and 3, we have the following (here $L' = L + 1$)

$$\frac{\lambda(EL')}{\lambda(ML)} = \frac{\lambda(EL')}{\lambda(EL)} \cdot \frac{\lambda(EL)}{\lambda(ML)} \approx 10^{-5} \times 10^{2} \approx 10^{-3}$$

$$\frac{\lambda(ML')}{\lambda(EL)} = \frac{\lambda(ML')}{\lambda(ML)} \cdot \frac{\lambda(ML)}{\lambda(EL)} \approx 10^{-5} \times 10^{-2} \approx 10^{-7}$$

You can thus see why $M2$ competes with $E1$ far less effectively than $E2$ competes with $M1$. Keep in mind, however, that these are only estimates based on some very crude approximations. The properties of specific nuclear states can modify these estimates by many orders of magnitude; for example, we often find cases in which $\lambda(E2) > \lambda(M1)$, especially in transitions between vibrational or rotational collective states.

10.5 ANGULAR DISTRIBUTION AND POLARIZATION MEASUREMENTS

In this section we consider the experimental techniques that help us to distinguish one multipole from another. Measuring the energy of a γ ray emitted in a certain transition gives us no information on the multipole character, and even if we know I_i and I_f, all we can do is restrict the range of possible L values, not determine how much of each is present. (In fact, more frequently the reverse process is used—we might know I_f and restrict the range of I_i by measuring L.) Even measuring the lifetime is of limited usefulness because of the many assumptions made in obtaining the Weisskopf estimates. To determine the multipole order of the γ radiation, we must measure the angular distribution of the radiation, and to distinguish electric from magnetic radiations, it is necessary to do additional measurements, such as to measure the polarization of the radiation.

By way of illustration, let us consider a dipole transition from $I_i = 1$ to $I_f = 0$. The initial state includes three sublevels with $m_i = +1, 0, -1$; the final state has only one sublevel, with $m_f = 0$. The angular distribution generally depends on the values of m_i and m_f. For example, in the case $m_i = 0$ to $m_f = 0$, the γ

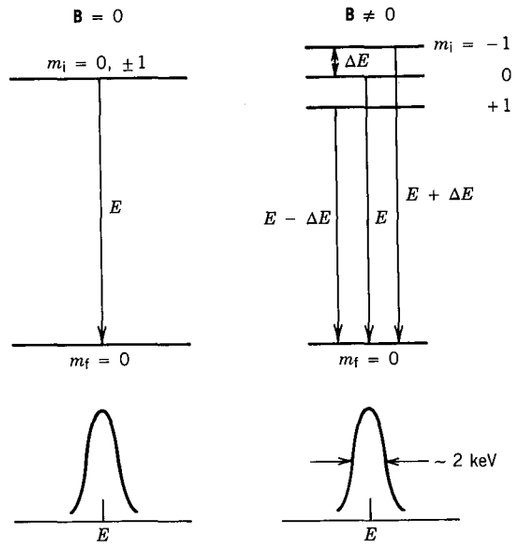

Figure 10.2 The nuclear Zeeman effect. In a magnetic field B, the $2I_i + 1$ sublevels of the state I_i are split into equally spaced states differing in energy by $\Delta E = \mu B / I_i$; for the case illustrated, $I_i = 1$, $2I_i + 1 = 3$, $I_f = 0$, and $\Delta E = \mu B$. Three transitions satisfy the dipole selection rule $\Delta m = 0, \pm 1$. The observed γ emission lines are shown below each diagram; because the energy resolution is much greater than the splitting ΔE, we cannot resolve the individual components.

emission probability varies as $\sin^2\theta$ (where the angle is defined with respect to the z axis that we use to measure the components of $\boldsymbol{I}_i$). This is in fact the quantum analog of the case of radiation from the classical dipole we considered in Section 10.2. The transitions from $m_i = \pm 1$ to $m_f = 0$ have angular distributions that vary as $\frac{1}{2}(1 + \cos^2\theta)$.

If we could pick out one of the three initial m states and measure the angular distribution of only that component of the transition, we would observe the characteristic angular distribution. The simplest scheme to do this would be to place the nuclei in a very strong magnetic field, so that the interaction of the magnetic moment μ of level I_i would give a splitting of that level depending on the relative orientations of $\boldsymbol{I}_i$ and the field $\boldsymbol{B}$. (This is exactly analogous to the Zeeman effect in atoms.) Figure 10.2 shows a representation of this situation. Before the field is turned on, there is one transition of energy E. When the field is present, the splitting of the levels gives three transitions of energy E, $E + \Delta E$, and $E - \Delta E$, where $\Delta E = \mu B$. If we could pick out only the component with energy $E + \Delta E$, for example, we would see the $\frac{1}{2}(1 + \cos^2\theta)$ distribution, relative to the direction of the field. We can estimate the magnitude of ΔE—for a typical magnetic moment of 1 nuclear magneton in a large field of 10 T, $\Delta E \simeq 10^{-6}$ eV. This small value of ΔE is far below the energy differences we can resolve with γ-ray detectors, which typically cannot separate or resolve transitions within 2 keV of each other. Thus what we actually observe is a mixture of all possible $m_i \to m_f$ ($+1 \to 0$, $0 \to 0$, $-1 \to 0$). If we let $W(\theta)$ represent the

observed angular distribution, then

$$W(\theta) = \sum_{m_i} p(m_i) W_{m_i \to m_f}(\theta)$$

where $p(m_i)$ is the *population* of the initial state, the fraction of the nuclei that occupies each sublevel.

Under normal circumstances all the populations are equal, $p(+1) = p(0) = p(-1) = \frac{1}{3}$, so that

$$W(\theta) \propto \tfrac{1}{3}\left[\tfrac{1}{2}(1 + \cos^2\theta)\right] + \tfrac{1}{3}(\sin^2\theta) + \tfrac{1}{3}\left[\tfrac{1}{2}(1 + \cos^2\theta)\right] = \text{constant}$$

that is, the angular distribution disappears and the radiation intensity is independent of direction.

There are two methods that can be used to create unequal populations $p(m_i)$ resulting in nonconstant $W(\theta)$. In the first method, we place the nuclei in a strong magnetic field, as we described previously, but at the same time we cool them to very low temperature, so low that the populations are made unequal by the Boltzmann distribution, $p(m_i) \propto e^{-m_i(\Delta E/kT)}$. To have unequal populations,

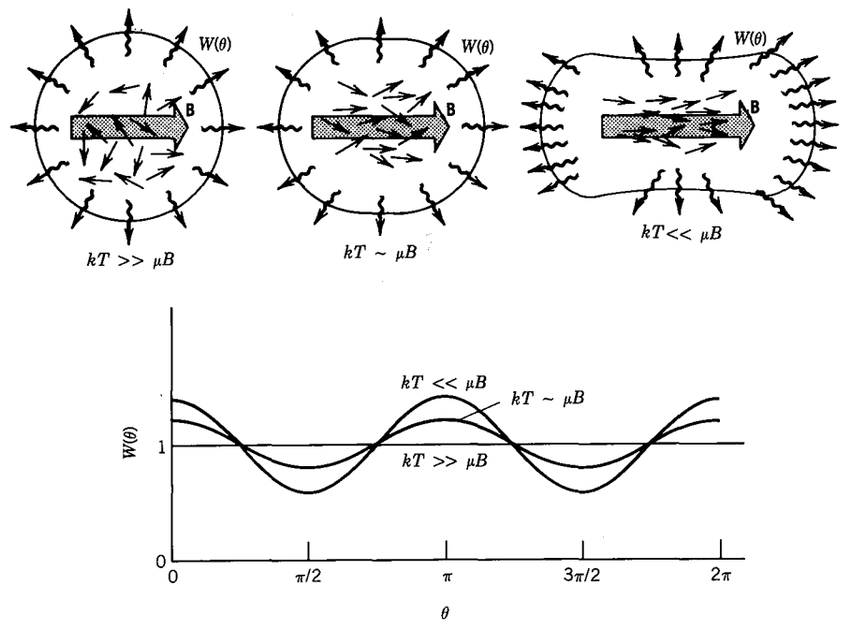

Figure 10.3 Angular distributions of nuclei with spins oriented at low temperatures. At top left is shown the distribution of radiation expected at high temperature; the magnetic field has essentially no effect in orienting the nuclear spins because of the thermal motion. At intermediate temperature (top center), the spins begin to align with the field, and the radiation distribution becomes nonuniform. At very low temperature, the spins are essentially completely aligned with the field. Measuring the angular distribution for dipole radiation would give the results shown at the bottom.

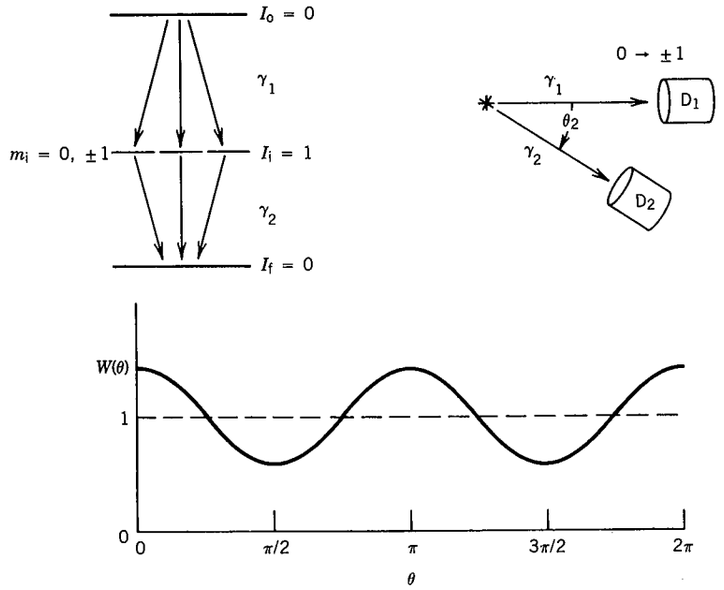

Figure 10.4 Angular correlation measurements. In a cascade of two radiations, here assumed to be $0 \rightarrow 1 \rightarrow 0$, the angular distribution of γ_2 is measured relative to the direction of γ_1. A typical result for two dipole transitions is shown at the bottom.

the exponential must be different from one, which means ΔE must be of the order of kT. (At high temperature, say room temperature, $kT \simeq 1/40$ eV, and $\Delta E \ll kT$, with the previous estimate of 10^{-6} eV for ΔE.) To have $\Delta E \sim kT$, we must cool the nuclei to $T \sim 0.01$ K. This is accomplished using continuously operating refrigerators, called helium dilution refrigerators, and this method, called low-temperature *nuclear orientation*, has become a powerful technique for determining γ-ray multipole characters and for inferring nuclear spin assignments. Figure 10.3 shows representative angular distributions for dipole radiation. Note that in this method we still cannot distinguish one component of the transition from another; we merely create a situation in which the various components contribute to the mixture with unequal weights.

The second method consists of creating an unequal mixture of populations $p(m_i)$ by observing a previous radiation. Let us assume for simplicity that the level I_i is populated by a transition from a state of spin $I_0 = 0$, so that there is a *cascade* $0 \rightarrow 1 \rightarrow 0$ of two radiations γ_1 and γ_2, as shown in Figure 10.4. Let's observe the first radiation in a certain direction, which we use to define the z axis; the second radiation is observed in a direction that makes an angle θ_2 with respect to the axis. With respect to the z axis, the first radiation has the same angular distribution we discussed above; for $m_0 = 0$ to $m_i = 0$, the distribution is proportional to $\sin^2\theta_1$ and for $m_0 = 0$ to $m_i = \pm 1$, to $\frac{1}{2}(1 + \cos^2\theta_1)$. Since we *define* the z axis by the direction of γ_1, it follows that $\theta_1 = 0$, and so the $0 \rightarrow 0$ transition cannot be emitted in that direction. That is, the nuclei for which γ_2 is observed following γ_1 must have a population of $p(m_i) = 0$ for $m_i = 0$. Thus the

angular distribution of γ_2 relative to γ_1 is

$$W(\theta) \propto \tfrac{1}{2}\left[\tfrac{1}{2}(1 + \cos^2\theta)\right] + 0(\sin^2\theta) + \tfrac{1}{2}\left[\tfrac{1}{2}(1 + \cos^2\theta)\right] \propto 1 + \cos^2\theta$$

This type of experiment is called an *angular correlation*; again, we do not observe the individual components of γ_2, but we create an unequal m-state population distribution of the state I_i.

We have considered these examples of angular distribution measurements for the simplest case of pure dipole radiation. In general, the angular distribution or correlation of multipole radiation is of the form of a polynomial in even powers of $\cos\theta$:

$$W(\theta) = 1 + \sum_{k=1}^{L} a_{2k} \cos^{2k}\theta \qquad (10.17)$$

where the coefficients a_{2k} depend on I_i, I_f, and L, and also on whether we are doing a low-temperature angular distribution or an angular correlation experiment. For example, for the angular correlation $4^+ \xrightarrow{\gamma_1} 2^+ \xrightarrow{\gamma_2} 0^+$, where γ_1 and γ_2 are $E2$ radiation (γ_2 is pure $E2$ by the selection rules (Equation 10.16); γ_1 has a negligible mixture of $M3$ and higher multipoles), $a_2 = \frac{1}{8}$ and $a_4 = \frac{1}{24}$, while for

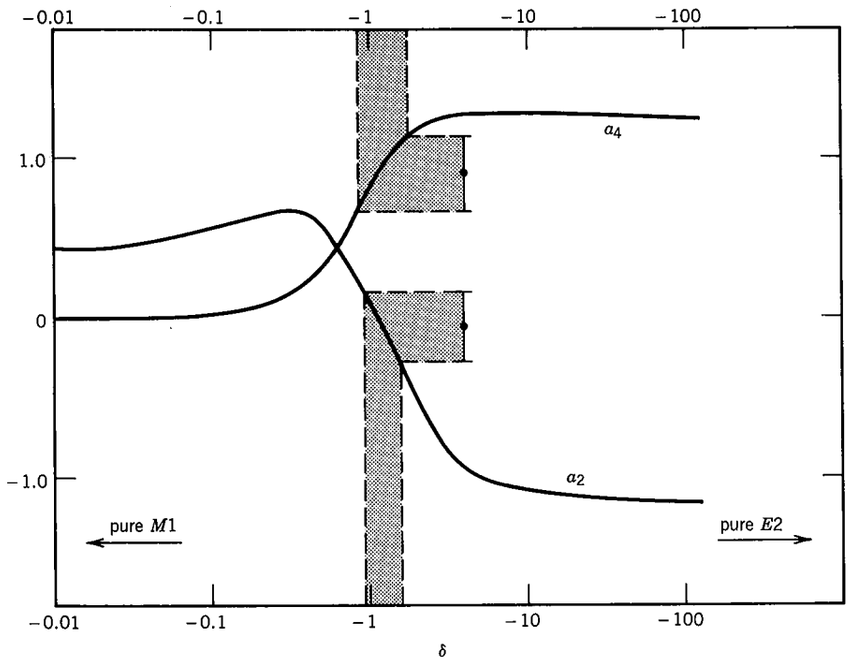

Figure 10.5 Analysis of angular correlation data for the ratio of $E2$ to $M1$ matrix elements in a transition. The vertical error bars show the ranges of the experimentally determined a_2 and a_4, each of which gives a corresponding value for δ. The a_2 and a_4 curves are derived from theory for this $2 \rightarrow 2 \rightarrow 0$ cascade in ^{110}Cd. Data from K. S. Krane and R. M. Steffen, *Phys. Rev. C* **2**, 724 (1970).

$0^+ \rightarrow 2^+ \rightarrow 0^+$ the angular correlation is $a_2 = -3$, $a_4 = 4$. Returning to the original goal of this discussion, let us consider the angular correlation for $2^+ \xrightarrow{\gamma_1} 2^+ \xrightarrow{\gamma_2} 0^+$, where γ_1 is a mixture of $M1$ and $E2$ (neglecting the higher multipoles). The coefficients a_2 and a_4 depend on the relative amounts of $M1$ and $E2$ radiation; Figure 10.5 shows a_2 and a_4 as they vary with the parameter δ, which essentially is $m_{fi}(E2)/m_{fi}(M1)$, where $m_{fi}(\sigma L)$ is the transition matrix element defined by Equation 10.9. The fraction of $E2$ radiation is $\delta^2/(1 + \delta^2)$ and the fraction of $M1$ radiation is $1/(1 + \delta^2)$. As an example, the case of the 818–658-keV $2^+ \rightarrow 2^+ \rightarrow 0^+$ cascade in ^{110}Cd has the measured values $a_2 = -0.06 \pm 0.22$, $a_4 = 0.89 \pm 0.24$. As shown in Figure 10.5, the deduced ratio of the multipole matrix elements is $\delta = -1.2 \pm 0.2$, corresponding to the 818-keV radiation being 59% $E2$ and 41% $M1$. This accurate knowledge of multipole character is extremely important in evaluating nuclear models and deducing partial lifetimes, as we discuss in Section 10.7. Thus angular distribution and correlation measurements have an extremely important role in nuclear spectroscopy.

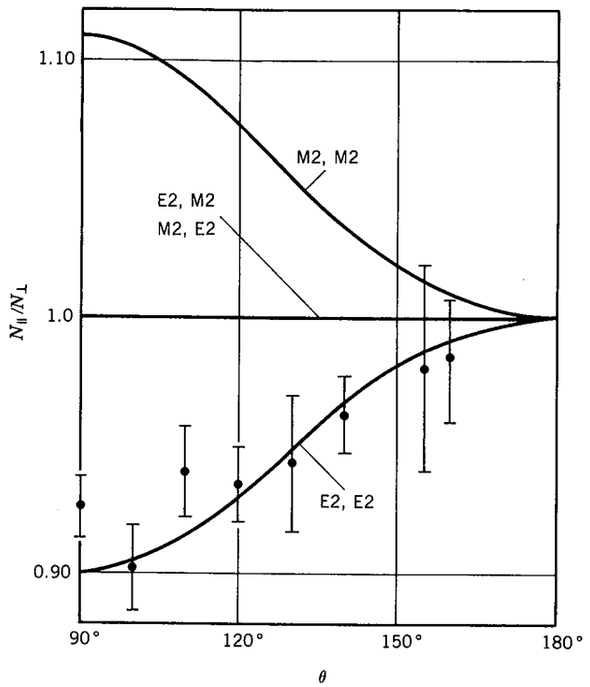

Figure 10.6 An angular correlation measurement in which the linear polarization of the radiation is measured. The angle θ refers, as in Figures 10.4 and 7.43, to the angle between the two radiations. Data shown are for two transitions in the decay of ^{46}Sc, obtained by F. Metzger and M. Deutsch, *Phys. Rev.* **78**, 551 (1950). Theoretical curves are drawn for various combinations of $E2$ and $M2$ radiations. The results indicate convincingly that both transitions must be of $E2$ character, consistent with the presently known $4^+ \rightarrow 2^+ \rightarrow 0^+$ level scheme.

To determine whether the radiation is electric or magnetic in character, additional measurements are necessary for in the angular distribution a_2 and a_4 are identical for E and M radiation. In Figure 10.1, you can see that the $\boldsymbol{E}$ vector of the radiation field is parallel to the dipole axis for electric radiation but normal to it for magnetic radiation. The same characteristic carries into the complete quantum description, and we can distinguish E from M radiation by determining the directional relationship between the axis of the emitting nucleus, the direction of the emitted radiation, and its $\boldsymbol{E}$ field. The plane formed by the radiation propagation direction $\boldsymbol{r}$ and the field $\boldsymbol{E}$ is called the *plane of polarization*. (Given $\boldsymbol{r}$ and $\boldsymbol{E}$, we can deduce $\boldsymbol{B}$ because the radiation propagates in the direction $\boldsymbol{E} \times \boldsymbol{B}$. Choosing $\boldsymbol{r}$ and $\boldsymbol{E}$ to define the polarization is merely a convention and has no intrinsic significance.) As in the previous measurement, we must begin with an unequal distribution of m states. (In the classical case, this would be equivalent to knowing the direction of the axis of the dipole since it is possible that a given direction for $\boldsymbol{E}$ can correspond to an electric dipole in the z direction or a magnetic dipole in the y direction.)

This type of measurement is called a *linear polarization distribution* and is usually accomplished by taking advantage of the polarization dependence of Compton scattering (see Section 7.9 and Figure 7.43). Figure 10.6 shows an example of an angular correlation in which the linear polarization of γ_2 is observed. As before, the observation of the previous radiation γ_1 in effect provides the unequal m-state distribution, and we measure the linear polarization of γ_2 by the intensity of the Compton-scattered photons as a function of ϕ.

10.6 INTERNAL CONVERSION

Internal conversion is an electromagnetic process that competes with γ emission. In this case the electromagnetic multipole fields of the nucleus do not result in the emission of a photon; instead, the fields interact with the atomic electrons and cause one of the electrons to be emitted from the atom. In contrast to β decay, the electron is not created in the decay process but rather is a previously existing electron in an atomic orbit. For this reason internal conversion decay rates can be altered slightly by changing the chemical environment of the atom, thus changing somewhat the atomic orbits. Keep in mind, however, that this is *not* a two-step process in which a photon is first emitted by the nucleus and then knocks loose an orbiting electron by a process analogous to the photoelectric effect; such a process would have a negligibly small probability to occur.

The transition energy ΔE appears in this case as the kinetic energy T_e of the emitted electron, less the binding energy B that must be supplied to knock the electron loose from its atomic shell:

$$T_e = \Delta E - B \tag{10.18}$$

As we did in our discussion of nuclear binding energy, we take B to be a positive number. The energy of a bound state is of course negative, and we regard the binding energy as that which we must supply to go from that state up to zero energy. Because the electron binding energy varies with the atomic orbital, for a

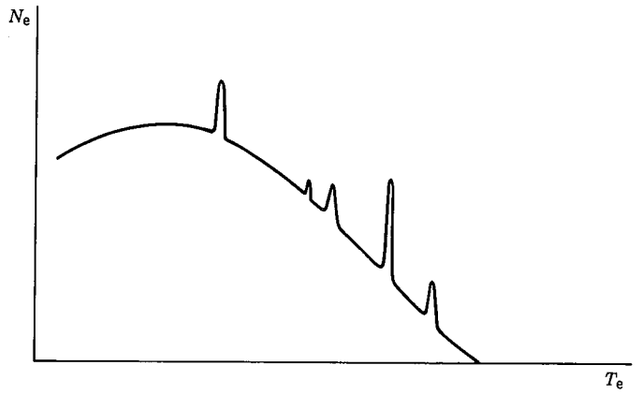

Figure 10.7 A typical electron spectrum such as might be emitted from a radioactive nucleus. A few discrete conversion electron peaks ride on the continuous background from β decay.

given transition ΔE there will be internal conversion electrons emitted with differing energies. The observed electron spectrum from a source with a single γ emission thus consists of a number of individual components; these are discrete components, however, and not at all continuous like the electrons emitted in β decay. Most radioactive sources will emit both β-decay and internal conversion electrons, and it is relatively easy to pick out the discrete conversion electron peaks riding on the continuous β spectrum (Figure 10.7).

Equation 10.18 suggests that the internal conversion process has a threshold energy equal to the electron binding energy in a particular shell; as a result, the conversion electrons are labeled according to the electronic shell from which they come: K, L, M, and so on, corresponding to principal atomic quantum numbers $n = 1, 2, 3, \ldots$. Furthermore, if we observe at very high resolution, we can even see the substructure corresponding to the individual electrons in the shell. For example, the L ($n = 2$) shell has the atomic orbitals $2s_{1/2}$, $2p_{1/2}$, and $2p_{3/2}$; electrons originating from these shells are called, respectively, L_I, L_{II}, and L_{III} conversion electrons.

Following the conversion process, the atom is left with a vacancy in one of the electronic shells. This vacancy is filled very rapidly by electrons from higher shells, and thus we observe characteristic X-ray emission accompanying the conversion electrons. For this reason, when we study the γ emission from a radioactive source we usually find X rays near the low-energy end of the spectrum.

As an illustration of the calculation of electron energies, consider the β decay of ^{203}Hg to ^{203}Tl, following which a single γ ray of energy 279.190 keV is emitted. To calculate the energies of the conversion electrons, we must look up the electron binding energies in the *daughter* Tl because it is from that atom that the electron emission takes place. (We will assume that the atomic shells have enough time to settle down between the β emission and the subsequent γ or conversion electron emission; this may not necessarily be true and will depend on the chemical environment and on the lifetime of the excited state.) Electron binding energies are conveniently tabulated in Appendix III of the *Table of Isotopes*. For Tl, we find the following:

$$B(\mathrm{K}) = 85.529 \text{ keV}$$
$$B(\mathrm{L_I}) = 15.347 \text{ keV}$$
$$B(\mathrm{L_{II}}) = 14.698 \text{ keV}$$
$$B(\mathrm{L_{III}}) = 12.657 \text{ keV}$$
$$B(\mathrm{M_I}) = 3.704 \text{ keV}$$

and so on through the M, N, and O shells. We therefore expect to find conversion electrons emitted with the following energies:

$$T_e(\mathrm{K}) = 279.190 - 85.529 = 193.661 \text{ keV}$$
$$T_e(\mathrm{L_I}) = 279.190 - 15.347 = 263.843 \text{ keV}$$
$$T_e(\mathrm{L_{II}}) = 279.190 - 14.698 = 264.492 \text{ keV}$$
$$T_e(\mathrm{L_{III}}) = 279.190 - 12.657 = 266.533 \text{ keV}$$
$$T_e(\mathrm{M_I}) = 279.190 - 3.704 = 275.486 \text{ keV}$$

Figure 10.8 shows the electron spectrum for ^{203}Hg. You can see the continuous β spectrum as well as the electron lines at the energies we have calculated.

One feature that is immediately apparent is the varying intensities of the conversion electrons from the decay. This variation, as we shall see, depends on the multipole character of the radiation field; in fact, measuring the relative probabilities of conversion electron emission is one of the primary ways to determine multipole characters.

In some cases, internal conversion is heavily favored over γ emission; in others it may be completely negligible compared with γ emission. As a general rule, it is necessary to correct for internal conversion when calculating the probability for γ emission. That is, if we know the half-life of a particular nuclear level, then the total decay probability λ_t (equal to $0.693/t_{1/2}$) has two components, one (λ_γ) arising from γ emission and another (λ_e) arising from internal conversion:

$$\lambda_t = \lambda_\gamma + \lambda_e \tag{10.19}$$

The level decays more rapidly through the combined process than it would if we considered γ emission alone. It is (as we shall see) convenient to define the *internal conversion coefficient* α as

$$\alpha = \frac{\lambda_e}{\lambda_\gamma} \tag{10.20}$$

That is, α gives the probability of electron emission relative to γ emission and ranges from very small (≈ 0) to very large. The total decay probability then becomes

$$\lambda_t = \lambda_\gamma(1 + \alpha) \tag{10.21}$$

We let α represent the *total* internal conversion coefficient and define *partial* coefficients representing the individual atomic shells:

$$\begin{aligned}\lambda_t &= \lambda_\gamma + \lambda_{e,K} + \lambda_{e,L} + \lambda_{e,M} + \cdots \\ &= \lambda_\gamma(1 + \alpha_K + \alpha_L + \alpha_M + \cdots)\end{aligned} \tag{10.22}$$

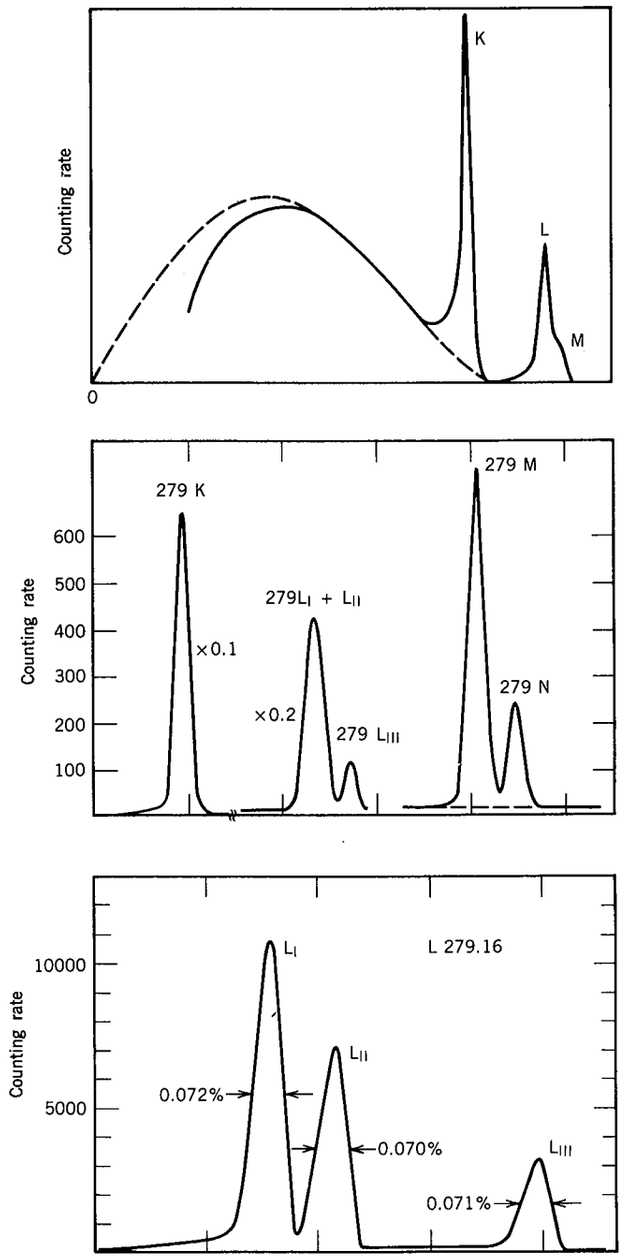

Figure 10.8 Electron spectrum from the decay of ^{203}Hg. At top, the continuous β spectrum can be seen, along with the K and unresolved L and M conversion lines. In the middle is shown the conversion spectrum at higher resolution; the L and M lines are now well separated, and even L_{III} is resolved. At yet higher resolution (bottom) L_I and L_{II} are clearly separated. *Sources*: (top) A. H. Wapstra et al., *Physica* **20**, 169 (1954); (middle) Z. Sujkowski, *Ark. Fys.* **20**, 243 (1961); (bottom) C. J. Herrlander and R. L. Graham, *Nucl. Phys.* **58**, 544 (1964).

and thus

$$\alpha = \alpha_K + \alpha_L + \alpha_M + \cdots \tag{10.23}$$

Of course, considering the subshells, we could break these down further, such as

$$\alpha_L = \alpha_{L_I} + \alpha_{L_{II}} + \alpha_{L_{III}} \tag{10.24}$$

and similarly for other shells.

The calculation of internal conversion coefficients is a difficult process, beyond the level of the present text. Let's instead try to justify some of the general results and indicate the way in which the calculation differs from the similar calculation for γ emission. Because the process is electromagnetic in origin, the matrix element that governs the process is quite similar to that of Equation 10.9 with two exceptions: the initial state includes a bound electron, so that $\psi_i = \psi_{i,N}\psi_{i,e}$ where N indicates the nuclear wave function and e indicates the electron wave function. Similarly, $\psi_f = \psi_{f,N}\psi_{f,e}$ where in this case $\psi_{f,e}$ is the free-particle wave function $e^{-i\mathbf{k}\cdot\mathbf{r}_e}$. To a very good approximation, the atomic wave function varies relatively little over the nucleus, and we can replace $\psi_{i,e}(\boldsymbol{r}_e)$ with its value at $\boldsymbol{r}_e = 0$. The important detail, however, is that all of the specifically nuclear information is contained in $\psi_{i,N}$ and $\psi_{f,N}$, and that the same electromagnetic multipole operator $m(\sigma L)$ governs both γ emission and internal conversion. The *nuclear* part of the matrix element of Equation 10.9 is therefore identical for both processes:

$$\lambda_\gamma(\sigma L) \propto |m_{fi}(\sigma L)|^2$$
$$\lambda_e(\sigma L) \propto |m_{fi}(\sigma L)|^2 \tag{10.25}$$

and thus the internal conversion coefficient α, the ratio of λ_e and λ_γ, is *independent* of the details of nuclear structure. The coefficient α will depend on the atomic number of the atom in which the process occurs, and on the energy of the transition and its multipolarity (hence, indirectly on the nuclear structure). We can therefore calculate and display general tables or graphs of α for different Z, T_e, and L.

We are oversimplifying here just a bit because the electron wave function $\psi_{i,e}$ does penetrate the nucleus and does sample the specific nuclear wave function, but it has a very slight, usually negligible, effect on the conversion coefficient.

A nonrelativistic calculation gives the following instructive results for electric (E) and magnetic (M) multipoles:

$$\alpha(EL) \cong \frac{Z^3}{n^3}\left(\frac{L}{L+1}\right)\left(\frac{e^2}{4\pi\epsilon_0\hbar c}\right)^4\left(\frac{2m_ec^2}{E}\right)^{L+5/2} \tag{10.26}$$

$$\alpha(ML) \cong \frac{Z^3}{n^3}\left(\frac{e^2}{4\pi\epsilon_0\hbar c}\right)^4\left(\frac{2m_ec^2}{E}\right)^{L+3/2} \tag{10.27}$$

In these expressions, Z is the atomic number of the atom in which the conversion takes place (the daughter, in the case of transitions following β decay) and n is the principal quantum number of the bound electron wave function; the factor $(Z/n)^3$ comes from the term $|\psi_{i,e}(0)|^2$ that appears in the conversion rate (the hydrogenic wave functions of Table 2.5 show the factor $(Z/n)^{3/2}$ in the nor-

malization constant). The dimensionless factor $(e^2/4\pi\epsilon_0\hbar c)$ is the fine structure constant with a value close to $\frac{1}{137}$.

These expressions for the conversion coefficients are only approximate, for the electron must be treated relativistically (transition energies are typically 0.5–1 MeV, so it is *not* true that $T_e \ll m_e c^2$) and the "point" nucleus Coulomb wave functions such as those of Table 2.5 do not properly take into account the important effects that occur when the electron penetrates the nucleus. Tabulations of conversion coefficients based on more rigorous calculations are listed at the end of the chapter. The approximate expressions do, however, illustrate a number of features of the conversion coefficients:

1. They increase as Z^3, and so the conversion process is more important for heavy nuclei than for light nuclei. For example, the 1.27-MeV $E2$ transition in $^{22}_{10}$Ne has $\alpha_K = 6.8 \times 10^{-6}$ and the 1.22-MeV $E2$ transition in $^{182}_{74}$W has $\alpha_K = 2.5 \times 10^{-3}$; their ratio is very nearly equal to $(10/74)^3$, as expected.
2. The conversion coefficient decreases rapidly with increasing transition energy. (In contrast, the probability for γ emission increases rapidly with energy.) For example, in ^{56}Co there are three $M1$ transitions, with energies 158 keV ($\alpha_K = 0.011$), 270 keV ($\alpha_K = 0.0034$), and 812 keV ($\alpha_K = 0.00025$). These decrease approximately as $E^{-2.5}$, as expected based on Equation 10.27.
3. The conversion coefficients increase rapidly as the multipole order increases; in fact, for the higher L values, conversion electron emission may be far more probable than γ emission. For example, in ^{99}Tc there is an $M1$ transition of 141 keV with $\alpha_K = 0.10$, while an $M4$ transition of 143 keV has $\alpha_K = 30$. Based on Equation 10.27 we would expect the ratio $\alpha_K(143)/\alpha_K(141)$ to be about $(2m_e c^2/E)^3$, or about 370, which is quite consistent with the observed ratio (about 300).
4. The conversion coefficients for higher atomic shells ($n > 1$) decrease like $1/n^3$. Thus for a given transition, we might roughly expect $\alpha_K/\alpha_L \simeq 8$. Using the correct electronic wave functions will cause this estimate to vary considerably, but many experimental values of α_K/α_L do fall in the range of 3–6, so even in this case our estimate serves us well.

We therefore expect relatively large K-shell conversion coefficients for low-energy, high-multipolarity transitions in heavy nuclei, with smaller values in other cases (higher atomic shells, higher transition energy, lighter nuclei, lower multipoles).

While these estimates give us reasonable qualitative values, for quantitative comparisons with experimental results, we must do detailed computations of the conversion coefficients, using the proper atomic wave functions. Figure 10.9 shows some results of such calculations. Notice that the coefficients differ considerably for EL and ML transitions; thus measurement of α allows us to determine the relative parities of nuclear states.

There is one other application for which internal conversion is an essential tool —the observation of $E0$ transitions, which are forbidden to go by electromagnetic radiation because the nuclear monopole moment (that is, its charge) cannot radiate to points external to the nucleus. The $E0$ transition is particularly important in decays from 0^+ initial states to 0^+ final states, which cannot occur

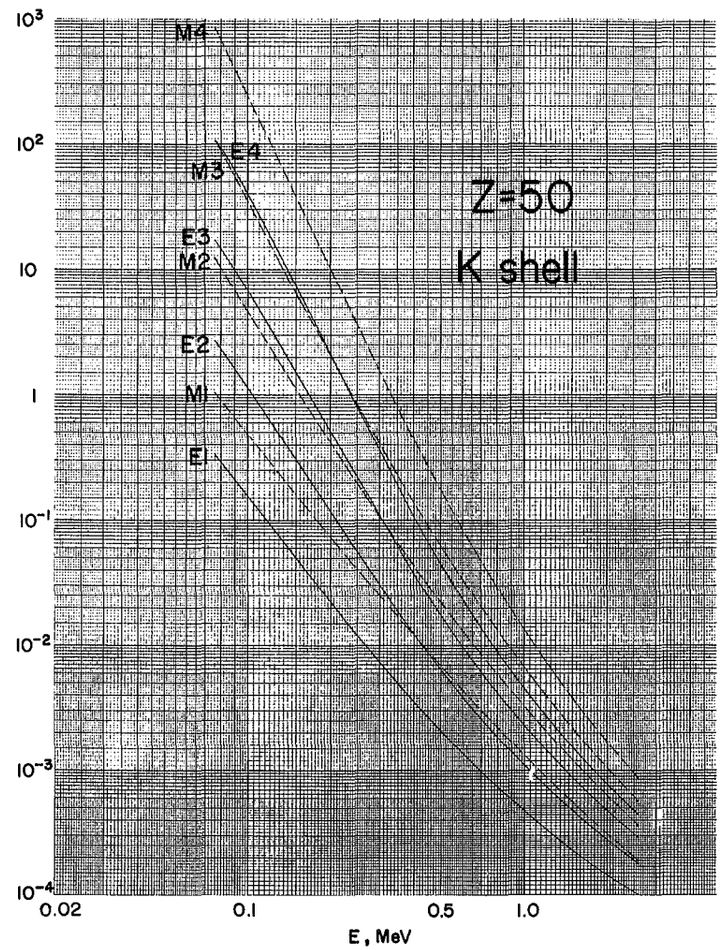

Figure 10.9 K-shell internal conversion coefficients for $Z = 50$. From *Table of Isotopes*, edited by C. M. Lederer and V. S. Shirley (New York: Wiley, 1978).

by any other direct process. We can regard the nucleus in this case as a spherically symmetric ball of charge; the only possible motion is a pulsation, which does not alter the electric field at points external to the sphere and thus produces no radiation. Electronic orbits that do not vanish near $r = 0$ (that is, s states) can sample the varying potential *within* the pulsating nucleus, and so a transfer of energy to the electron is possible.

Because no γ rays are emitted, it is not possible to define a conversion coefficient (α is infinite for $\lambda_\gamma = 0$). We can illustrate a particular case in which the decay occurs by the ^{72}Ge level scheme shown in Figure 10.10. The excited 0^+ state decays to the ground state by $E0$ conversion with a half-life of 0.42 μs. The nearby 2^+ state can decay by γ emission much more rapidly; the internal conversion coefficient for that decay is only 4.9×10^{-4}. Comparison of these rates will involve evaluating the nuclear matrix elements (because we cannot take

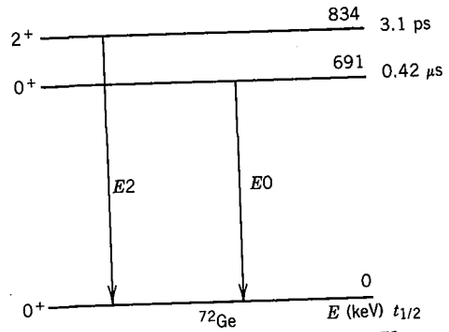

Figure 10.10 Energy levels in ^{72}Ge.

the ratio λ_e/λ_γ for the $E0$ transition, its matrix elements do not cancel), but may reveal to us something about the internal structure of the excited 0^+ state.

10.7 LIFETIMES FOR γ EMISSION

In Chapter 7, we discussed techniques for measuring the half-lives of excited states. One primary usefulness of these experimental values is for comparing with theoretical values calculated on the basis of different models of the nucleus. If we compare various calculated values with the experimental one, we can often draw some conclusions about the structure of the nucleus.

Before we do this, we must first evaluate the *partial* decay rate for γ emission, as we did at the end of Section 6.5. Let's consider the example of the decay shown in Figure 10.11. The half-life of the 1317-keV level has been measured to be 8.7 ps. Its total decay constant is therefore

$$\lambda_t = \frac{0.693}{t_{1/2}} = \frac{0.693}{8.7 \times 10^{-12}\ \text{s}} = 8.0 \times 10^{10}\ \text{s}^{-1}$$

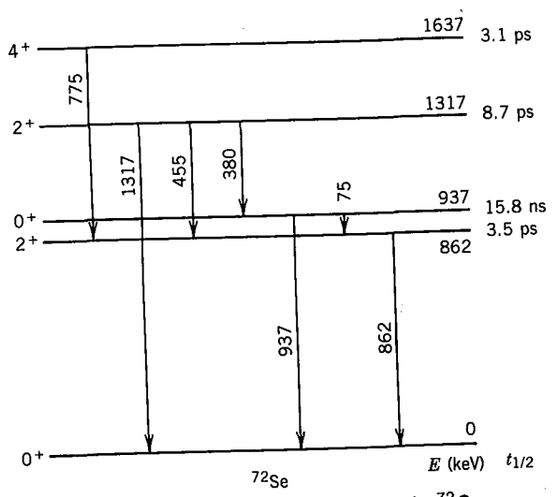

Figure 10.11 Energy levels in ^{72}Se.

This decay rate is just the sum of the decay rates of the three transitions that depopulate the state:

$$\lambda_t = \lambda_{t,1317} + \lambda_{t,455} + \lambda_{t,380}$$
$$= \lambda_{\gamma,1317}(1 + \alpha_{1317}) + \lambda_{\gamma,455}(1 + \alpha_{455}) + \lambda_{\gamma,380}(1 + \alpha_{380})$$

The conversion coefficients can be found in standard reference works (they have not been measured in this case) and are sufficiently small (< 0.01) that they can be neglected (compared with 1) to the precision of this calculation. Thus

$$\lambda_t = \lambda_{\gamma,1317} + \lambda_{\gamma,455} + \lambda_{\gamma,380}$$

The relative intensities of the three γ rays have been measured to be

$$\lambda_{\gamma,1317} : \lambda_{\gamma,455} : \lambda_{\gamma,380} = 51 : 39 : 10$$

and so the partial decay rates for the three γ rays are

$$\lambda_{\gamma,1317} = 0.51(8.0 \times 10^{10}\ \text{s}^{-1}) = 4.1 \times 10^{10}\ \text{s}^{-1}$$
$$\lambda_{\gamma,455} = 0.39(8.0 \times 10^{10}\ \text{s}^{-1}) = 3.1 \times 10^{10}\ \text{s}^{-1}$$
$$\lambda_{\gamma,380} = 0.10(8.0 \times 10^{10}\ \text{s}^{-1}) = 0.80 \times 10^{10}\ \text{s}^{-1}$$

It is these *partial rates for γ emission* that can be compared with calculated values, such as the Weisskopf estimates of Equation 10.13. Let us calculate the expected values of $\lambda(E2)$:

$$\lambda_{E2,1317} = 8.7 \times 10^{10}\ \text{s}^{-1}$$
$$\lambda_{E2,455} = 4.3 \times 10^{8}\ \text{s}^{-1}$$
$$\lambda_{E2,380} = 1.7 \times 10^{8}\ \text{s}^{-1}$$

The case of the 937-keV level ($t_{1/2} = 15.8$ ns) can be handled similarly:

$$\lambda_t = \frac{0.693}{15.8\ \text{ns}} = 4.39 \times 10^{7}\ \text{s}^{-1}$$
$$\lambda_t = \lambda_{t,937} + \lambda_{t,75}$$
$$= \lambda_{e,937} + \lambda_{\gamma,75}(1 + \alpha_{75})$$

because the 937-keV transition is of the $0 \rightarrow 0$, $E0$ type we discussed in the previous section. The total conversion coefficient of the 75-keV transition is about 2.4 (from tables or graphs). Experimentally, it is known that $\lambda_{\gamma,75} : \lambda_{e,937} = 73 : 27$, and thus

$$\lambda_{e,937} = 4.3 \times 10^{6}\ \text{s}^{-1}$$
$$\lambda_{\gamma,75} = 1.16 \times 10^{7}\ \text{s}^{-1}$$

Finally, for the 862-keV transition, we find

$$\lambda_{\gamma,862} = 2.0 \times 10^{11}\ \text{s}^{-1}$$

From the Weisskopf estimates, we would compute

$$\lambda_{E2,75} = 5.2 \times 10^{4}\ \text{s}^{-1}$$
$$\lambda_{E2,862} = 1.0 \times 10^{10}\ \text{s}^{-1}$$

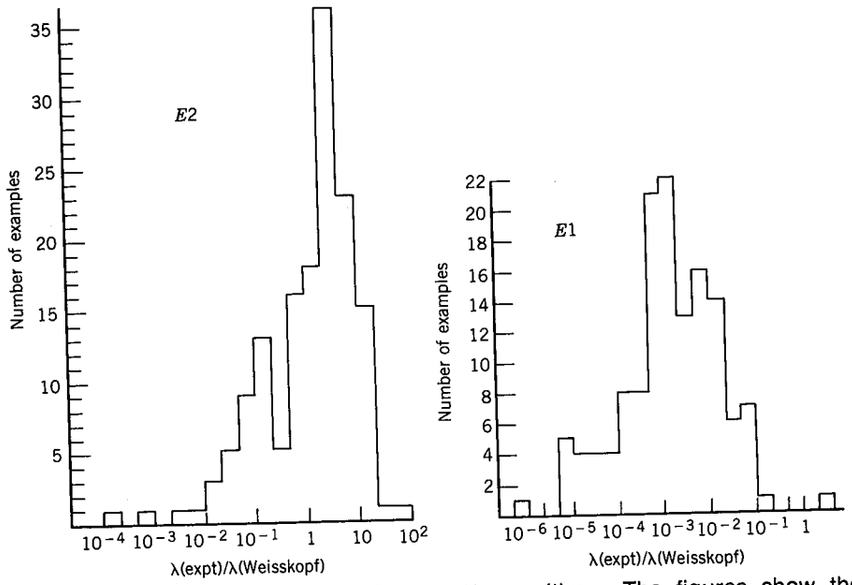

Figure 10.12 Systematics of $E2$ and $E1$ transitions. The figures show the number of cases versus the ratio between the observed decay rate and the value calculated from the Weisskopf formulas. From S. J. Skorka et al., *Nucl. Data* **2**, 347 (1966).

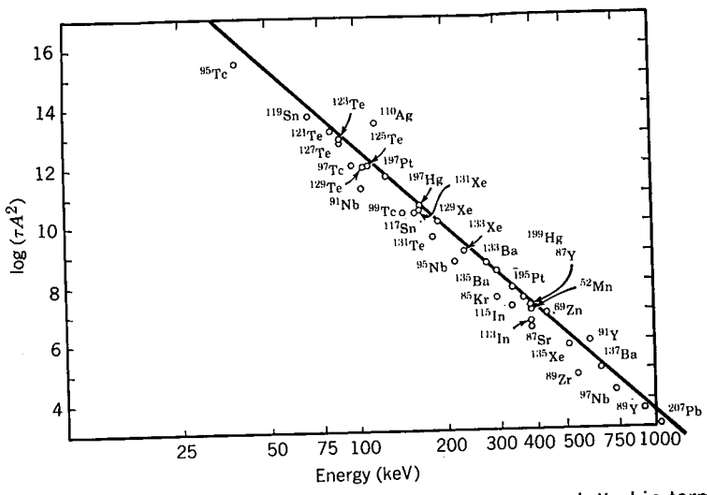

Figure 10.13 Systematics of $M4$ transitions. The data are plotted in terms of the mean life (the reciprocal of the decay constant λ). The straight line is determined from Equation 10.15. Note especially the good agreement between the data points and the expected E^{-9} dependence. From M. Goldhaber and A. W. Sunyar, *Phys. Rev.* **83**, 906 (1951).

One feature that generally emerges from these calculations is that the measured transition rates are frequently at least an order of magnitude larger than the Weisskopf estimates for $E2$ transitions. This is strong evidence for the *collective* aspects of nuclear structure discussed in Chapter 5—the Weisskopf estimates are based on the assumption that the transition arises from the motion of a *single nucleon*, and the fact that these are too small indicates that *many* nucleons must be taking part in the transition. Figure 10.12 summarizes similar results for many $E2$ transitions, and you can see that this enhancement or acceleration of the single-particle $E2$ rate is quite a common feature. No such effect occurs for $E1$ transitions, which are generally slower than the single-particle rates. On the other hand, consider Figure 10.13 which shows the systematic behavior of $M4$ transitions. Here the agreement between theory and experiment is excellent.

10.8 GAMMA-RAY SPECTROSCOPY

The study of the γ radiations emitted by radioactive sources is one of the primary means to learn about the structure of excited nuclear states. Gamma-ray detection is relatively easy to accomplish, and can be done at high resolution (transitions a mere 2 keV apart can be cleanly separated by good γ detectors) and with high precision (uncertainties of a few eV in typical cases and more than an order of magnitude better in the best cases). Knowledge of the locations and properties of the excited states is essential for the evaluation of calculations based on any nuclear model, and γ-ray spectroscopy is the most direct, precise, and often the easiest way to obtain that information.

Let's consider how the "ideal" γ-ray experiments might proceed to provide us with the information we need about nuclear excited states:

1. A spectrum of the γ rays shows us the energies and intensities of the transitions.
2. Coincidence measurements give us clues about how these transitions might be arranged among the excited states.
3. Measuring internal conversion coefficients can give clues about the character of the radiation and the relative spins and parities of the initial and final states. Additional clues may come from angular distribution and correlation measurements.
4. Absolute transition probabilities can be found by determining the half-lives of the levels.

As a first example, we consider the decay of ^{108m}Ag ($t_{1/2}$ = 127 y). Figure 10.14 shows the conversion electron and γ-ray spectra, and Table 10.1 shows the deduced relative γ and electron intensities.

The first excited state of ^{108}Pd is known from many nuclear reaction studies to be at an energy of 434 keV and to be a 2^+ state, as in nearly all even-Z, even-N nuclei. We therefore recognize the 434-keV transition shown in Table 10.1 as representing the decay of this state, and we assume the transition to be a pure $E2$, $2^+ \rightarrow 0^+$ transition. From conversion coefficient tables, we can determine that the theoretical conversion coefficients are $\alpha_K(434) = 7.89 \times 10^{-3}$, $\alpha_{L+M+\cdots} = 1.0 \times 10^{-3}$. Given the intensities from Table 10.1, the remaining conversion

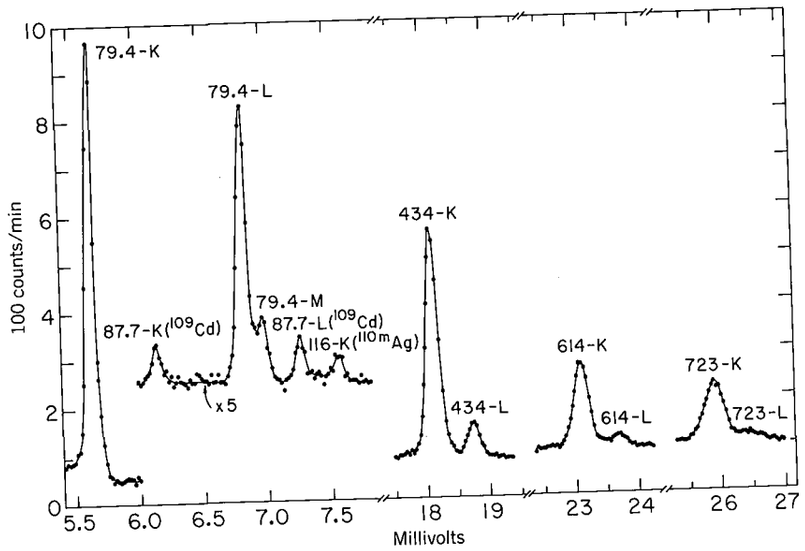

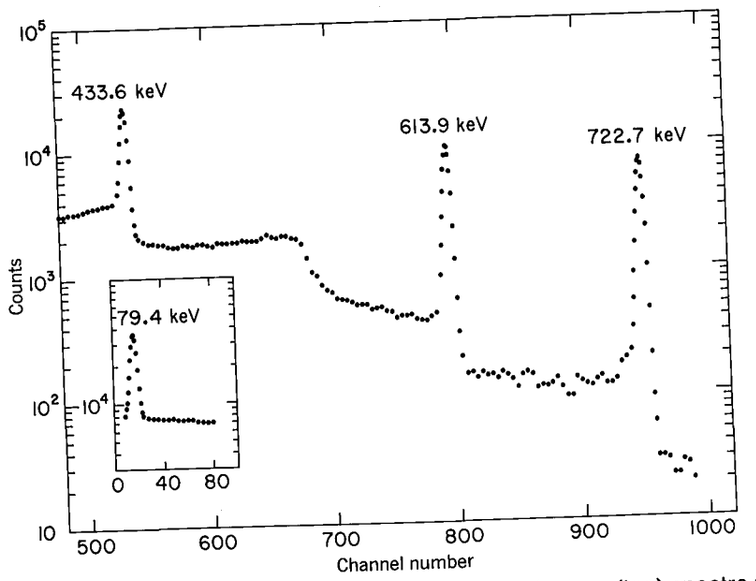

Figure 10.14 Gamma-ray (bottom) and conversion electron (top) spectra following the ^{108m}Ag decay. The γ spectrum was obtained with a Ge(Li) detector. The electron spectrum, obtained with a magnetic spectrometer, shows the high resolution necessary to separate the K and L lines. From O. C. Kistner and A. W. Sunyar, *Phys. Rev.* **143**, 918 (1966).

Table 10.1 Conversion Electron and γ-Ray Intensities of Transitions Following the Decay of ^{108m}Ag

Transition Energy (keV)	Relative γ Intensity	Relative Electron Intensity	Conversion Coefficient (units of 10^{-3})	
			Experimental	Theoretical
79.2	7.3 ± 0.8	204 ± 10 (K)	220 ± 26	270 (*E*1), 710 (*M*1), 2400 (*E*2)
		25 ± 2 (L)	27 ± 4	33 (*E*1), 88 (*M*1), 777 (*E*2)
434.0	≡ 100	≡ 100 (K)	≡ 7.89	7.89 (*E*2)
		14.8 ± 2.3 (L + ⋯)	1.17 ± 0.18	1.02 (*E*2)
614.4	103 ± 3	37 ± 3 (K)	2.83 ± 0.24	1.03 (*E*1), 3.01 (*M*1), 2.92 (*E*2)
		5.1 ± 1.6 (L + ⋯)	0.39 ± 0.12	0.12 (*E*1), 0.35 (*M*1), 0.36 (*E*2)
632.9	0.16 ± 0.02			
723.0	102 ± 3	25.0 ± 1.2 (K)	1.93 ± 0.11	0.72 (*E*1), 2.06 (*M*1), 1.91 (*E*2)
		4.6 ± 0.8 (L + ⋯)	0.35 ± 0.06	0.08 (*E*1), 0.24 (*M*1), 0.23 (*E*2)

Source: Experimental data from O. C. Kistner and A. W. Sunyar, *Phys. Rev.* **143**, 918 (1966).

coefficients can be computed in the following way:

$$\alpha_K(434) = \frac{I_K(434)}{I_\gamma(434)}$$

$$\alpha_K(614) = \frac{I_K(614)}{I_\gamma(614)}$$

where I represents the tabulated intensities.

Since we have *relative*, rather than *absolute*, intensities, we form the ratio

$$\frac{\alpha_K(614)}{\alpha_K(434)} = \frac{I_K(614)}{I_K(434)} \cdot \frac{I_\gamma(434)}{I_\gamma(614)}$$

$$\alpha_K(614) = \alpha_K(434) \cdot \frac{I_K(614)}{I_K(434)} \cdot \frac{I_\gamma(434)}{I_\gamma(614)}$$

$$= 7.89 \times 10^{-3} \cdot \frac{37 \pm 3}{100} \cdot \frac{100}{103 \pm 3}$$

$$= (2.83 \pm 0.24) \times 10^{-3}$$

From a similar procedure, the remaining conversion coefficients can be calculated, as listed in Table 10.1, and from tabulated values, we can find the theoretical values also listed in the table.

The 614- and 723-keV transitions are either $M1$ or $E2$ character, but from the conversion coefficients we cannot decide which is correct because it happens (for this atomic number and γ-ray energy range) the $M1$ and $E2$ values are nearly equal.

Further information can be obtained from coincidence experiments, illustrated in Figure 10.15. The low-energy end of the electron spectrum shows another

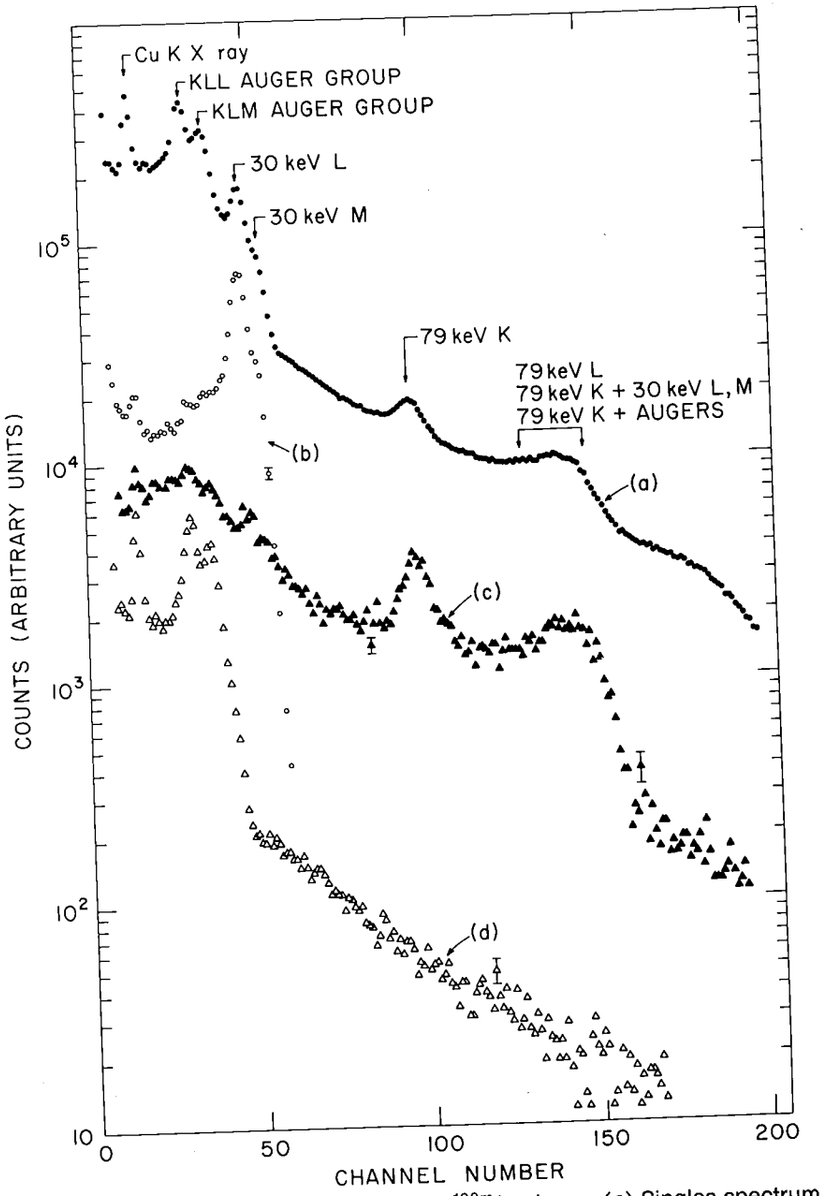

Figure 10.15 Coincidence spectra in the ^{108m}Ag decay. (*a*) Singles spectrum for comparison. (*b*) Spectrum in coincidence with 79-keV γ ray. (*c*) Spectrum in coincidence with K X rays. (*d*) Spectrum in coincidence with 434-, 614-, and 723-keV γ's. From O. C. Kistner and A. W. Sunyar, *Phys. Rev.* **143**, 918 (1966).

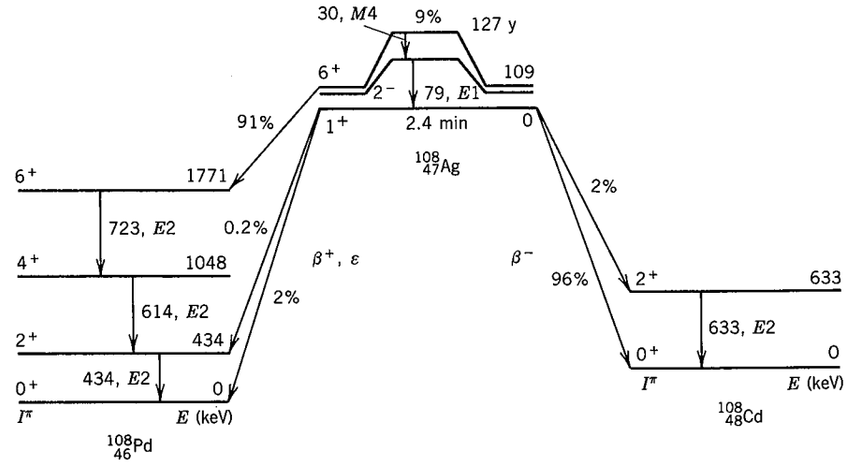

Figure 10.16 Decay scheme of ^{108}Ag. The 127-y isomer decays 91% by β decay and 9% through γ rays. The branching ratios of the β decay of the 2.4-min ground state are also shown.

transition, of energy 30.4 keV; its γ intensity is too low to be observed, but from the relative subshell intensities $L_I/(L_{II} + L_{III})$ it is deduced to be of $M4$ character. Neither this transition nor the 79.2-keV transition are in coincidence with the 434-, 614-, or 723-keV transitions. This strongly suggests that the 30.4- and 79.2-keV transitions take place in ^{108}Ag following the decay of the isomer. Furthermore, the coincidence relationship among the 434-, 614-, and 723-keV transitions suggests that they follow one another in cascade.

The resulting decay scheme deduced on the basis of these (and other) data is shown in Figure 10.16. The spins of the 1048- and 1771-keV levels are deduced from angular correlation and linear polarization measurements, and the transitions are then of $E2$ multipolarity. The 633-keV transition is deduced to take place in ^{108}Cd, and must follow the decay of the ^{108}Ag ground state. (Otherwise, the β decay would be $6^+ \rightarrow 2^+$, a fourth-forbidden process not likely to be observed.)

The 127-y isomeric state decays 91% by an allowed β decay to the 6^+ state in ^{108}Pd, which then decays through the cascade of three transitions. Because there is negligible β feeding of the 4^+ or 2^+ levels (the 2^+ level is fed by only 0.2% of 9% of the decays), the three transitions should all have the same total (γ plus electron) intensity, as can be confirmed from the data of Table 10.1. The ^{108}Ag ground state decays through four different allowed β branches, with a half-life of 2.4 min.

As a second example, we consider the decay of isomeric ^{180m}Hf. A γ-ray spectrum is shown in Figure 10.17, and the deduced γ intensities and conversion coefficients are shown in Table 10.2. The conversion coefficients of the 93-, 215-, 332-, and 443-keV transitions strongly suggest $E2$ multipolarity, while for 57- and 501-keV, they suggest $E1$ and $E3$, respectively.

Since ^{180}Hf is an even-Z, even-N nucleus, we expect the first excited state to be a 2^+ state, and such a state has been identified at 93 keV from a variety of experiments. In this region, we expect the sequence of $0^+, 2^+, 4^+, 6^+, \ldots$ rota-

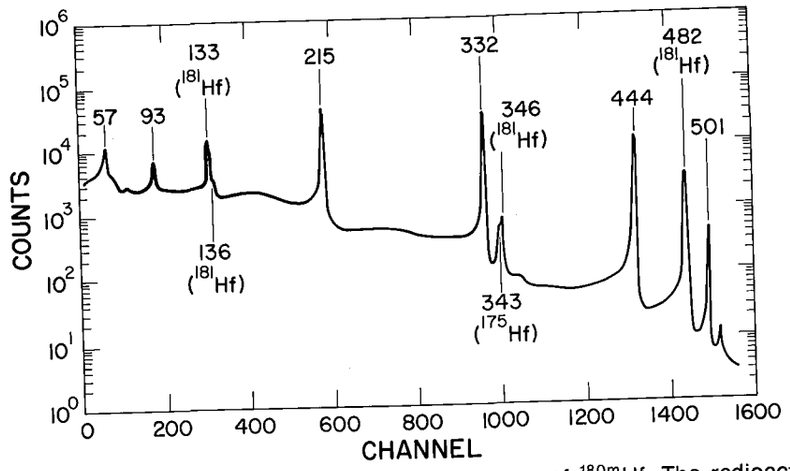

Figure 10.17 Gamma ray spectrum from the decay of ^{180m}Hf. The radioactive sample was made by neutron activation, which also produced other isotopes of Hf; γ rays from these other isotopes are labeled.

tional states with characteristic $I(I+1)$ spacing, and so we expect to find a 4^+ state at an energy of $\frac{10}{3}$ of the 2^+ energy, or 310 keV, with a 4^+–2^+ transition of energy $310 - 93 = 217$ keV. This is presumably the 215-keV $E2$ transition seen in the γ spectrum. The 6^+ state is expected at 651 keV, and the 6^+–4^+ transition should be of energy $651 - 310 = 341$ keV, which we identify with the observed 332-keV transition. The 8^+ energy is expected to be 1116 keV, and the 8^+–6^+ transition ($1116 - 651 = 465$ keV) we guess to be the observed 443 keV. To place the 57- and 501-keV transitions, we notice the energy sum $57.5 + 443.2 = 500.7$, which strongly suggests that a level 57.5 keV above the 8^+ level emits both the 57.5- and 500.7-keV transitions, with the 500.7-keV transition proceeding directly to the 6^+ state in parallel with the cascade $57.5 + 443.2$ keV. To check this assumption, we examine the total intensities of the transitions, which we find, according to Equation 10.21, by $I_T = I_\gamma(1 + \alpha)$, where α is the *total* conversion coefficient (the sum of the individual coefficients). From the data of Table 10.2, the following relative intensities can be computed:

$$I_T(57.5) = 87.1 \pm 2.9 \qquad I_T(332.3) = 105.3 \pm 1.1$$
$$I_T(93.3) = 108.1 \pm 4.8 \qquad I_T(443.2) = 89.7 \pm 1.6$$
$$I_T(215.3) = 103.4 \pm 1.0 \qquad I_T(500.7) = 16.2 \pm 0.4$$

Note that, within the uncertainties, $I_T(93.3) = I_T(215.3) = I_T(332.3)$, as expected for transitions emitted in a cascade, one following the other. The 443.2 intensity is smaller, suggesting an alternative branch to the 6^+ state other than through the 443.2-keV, 8^+–6^+ transition, consistent with the assumption that the 500.7-keV transition goes to the 6^+ state. Finally, note that $I_T(57.5) = I_T(443.2)$, suggesting they are in cascade, and that $I_T(57.5) + I_T(500.7) = I_T(332.3)$, suggesting the two branches that feed the 6^+ level, one by the 57.5-keV transition and another by the 500.7-keV transition.

Table 10.2 Gamma Decays of ^{180m}Hf

Transition Energy (keV)	Relative γ Intensity	Conversion Coefficient: Experiment (atomic shell)	Conversion Coefficient: Theory (multipole)
57.5	51.3 ± 1.2	0.430 ± 0.029 (L)	0.452 ($E1$)
		0.083 ± 0.007 (M)	0.105 ($E1$)
		0.023 ± 0.004 (N + ⋯)	0.031 ($E1$)
93.3	17.6 ± 0.4	≡ 1.10 (K)	1.10 ($E2$)
		3.13 ± 0.19 (L)	2.72 ($E2$)
		0.91 ± 0.11 (M + ⋯)	0.85 ($E2$)
215.3	86.2 ± 0.8	0.123 ± 0.009 (K)	0.14 ($E2$)
		0.077 ± 0.011 (L)	0.071 ($E2$)
332.3	≡ 100.0 ± 1.0	0.038 ± 0.003 (K)	0.042 ($E2$)
		0.015 ± 0.002 (L)	0.013 ($E2$)
443.2	87.7 ± 1.6	0.0189 ± 0.0017 (K)	0.020 ($E2$)
		0.0044 ± 0.0007 (L)	0.005 ($E2$)
500.7	15.4 ± 0.4	0.037 ± 0.012 (K)	0.124 ($M2$), 0.038 ($E3$)
		0.016 ± 0.005 (L)	0.062 ($M2$), 0.016 ($E3$)

Source: Data for this table came from various sources compiled in the *Nuclear Data Sheets* **15**, 559 (1975).

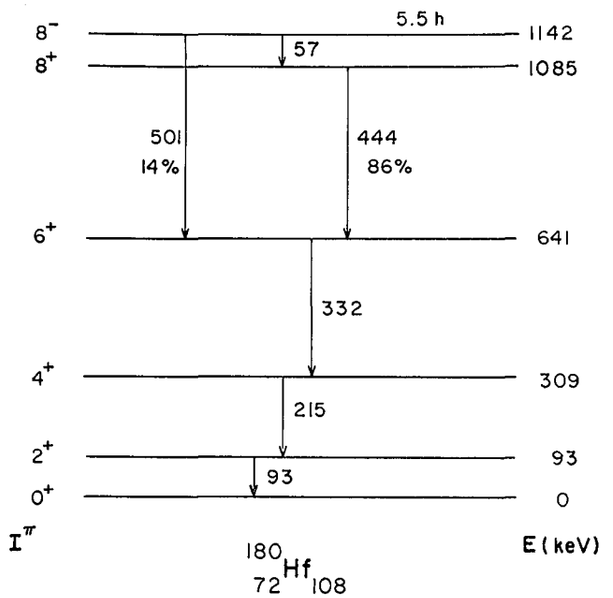

Figure 10.18 The isomeric decay of ^{180m}Hf.

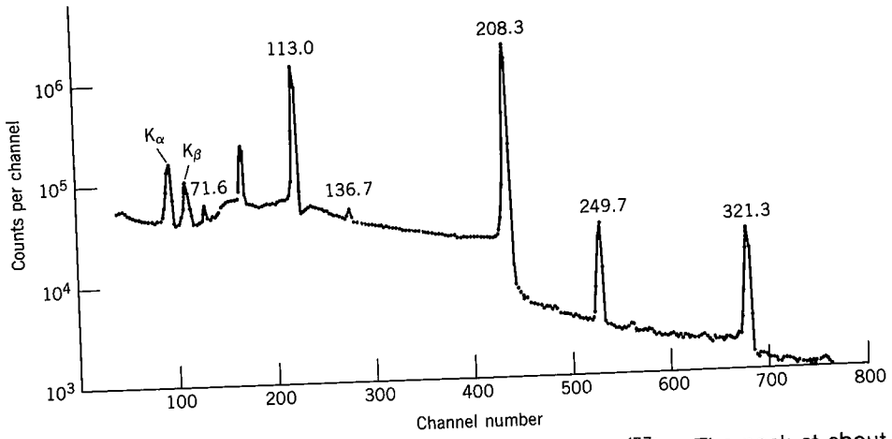

Figure 10.19 Gamma-ray spectrum from the decay of ^{177}Lu. The peak at about 90 keV is from an impurity activity produced in this neutron-activated sample. (Data from the author's laboratory.)

The parity of the level that emits the 57.5- and 500.7-keV transitions must be negative (because of their $E1$ and $E3$ characters, respectively), and its spin must be 7, 8, or 9 to permit decay to 8^+ via the $E1$ transition. We can eliminate the 7^- possibility because it would allow the 500.7-keV transition to 6^+ to be of $E1$ character, and 9^- can be eliminated by angular correlation experiments, which show the 500.7-keV transition to have a small ($\approx 3\%$) $M2$ component, which the conversion coefficients are not sensitive enough to reveal.

The resulting decay scheme is shown in Figure 10.18. Of course, many additional measurements are required to confirm that our guesses based on the γ

Table 10.3 γ Transitions in the Decay of ^{177}Lu

Transition Energy (keV)	Relative γ Intensity	Conversion Coefficient: Experiment (atomic shell)	Conversion Coefficient: Theory (multipole)
71.6	2.4 ± 0.1	0.90 ± 0.11 (K)	0.72 ($E1$), 92.0 ($M2$)
		0.087 ± 0.010 (L_1)	0.071 ($E1$), 24.3 ($M2$)
113.0	≡ 100	0.78 ± 0.05 (K)	2.4 ($M1$), 0.74 ($E2$)
		0.091 ± 0.011 (L_1)	0.345 ($M1$), 0.076 ($E2$)
136.7	0.92 ± 0.06	0.49 ± 0.08 (K)	1.45 ($M1$), 0.48 ($E2$)
		0.08 ± 0.02 (L_1)	0.20 ($M1$), 0.05 ($E2$)
208.3	164 ± 10	0.046 ± 0.004 (K)	0.046 ($E1$), 2.05 ($M2$)
		0.0063 ± 0.0006 (L_1)	0.0053 ($E1$), 0.38 ($M2$)
249.7	3.0 ± 0.2	0.101 ± 0.009 (K)	0.26 ($M1$), 0.094 ($E2$)
321.3	3.6 ± 0.2	0.102 ± 0.013 (K)	0.0155 ($E1$), 0.49 ($M2$)
		0.017 ± 0.002 (L_1)	0.0018 ($E1$), 0.081 ($M2$)

Sources: Gamma-ray data from A. J. Haverfield et al., *Nucl. Phys. A* **94**, 337 (1967). Electron conversion data from A. P. Agnihotry et al., *Phys. Rev. C* **9**, 336 (1974).

decays are in fact correct. The 5.5-h half-life is one of the longest known for γ-emitting isomers.

For our final example, we consider the 6.7-day decay of ^{177}Lu. The γ-ray spectrum is shown in Figure 10.19 and the γ and conversion data are listed in Table 10.3. The β decays of ^{177}Lu to ^{177}Hf were discussed in Section 9.10; there are four decays, leading to the ground state and to excited states at 113, 250, and 321 keV. Transitions from each of these states to the ground state can be seen among those listed in Table 10.3, and we therefore assume the excited states to be at energies of 113.0, 249.7, and 321.3 keV. (These γ energies are determined to about ± 0.1 keV, while the β energies are determined only to ± 2–3 keV.) We also find in the transitions of Table 10.3 all possible transitions connecting the excited states:

$$321.3 - 249.7 \text{ keV} = 71.6 \text{ keV}$$
$$321.3 - 113.0 \text{ keV} = 208.3 \text{ keV}$$
$$249.7 - 113.0 \text{ keV} = 136.7 \text{ keV}$$

The ground state and first two excited states of ^{177}Hf are known to be the lowest states of a rotational band with spins $\frac{7}{2}^-, \frac{9}{2}^-, \frac{11}{2}^-, \ldots$. We would expect the 113.0-keV transition to be $\frac{9}{2}^- \rightarrow \frac{7}{2}^-$ and thus of $M1 + E2$ character, the 136.7-keV transition to be $\frac{11}{2}^- \rightarrow \frac{9}{2}^-$ and likewise $M1 + E2$, and the 249.7-keV transition to be $\frac{11}{2}^- \rightarrow \frac{7}{2}^-$ $E2$. These expectations are consistent with the conversion coefficients. The 321.3 level decays to all three lower levels through $E1 + M2$ transitions, and thus only a $\frac{9}{2}^+$ assignment is possible.

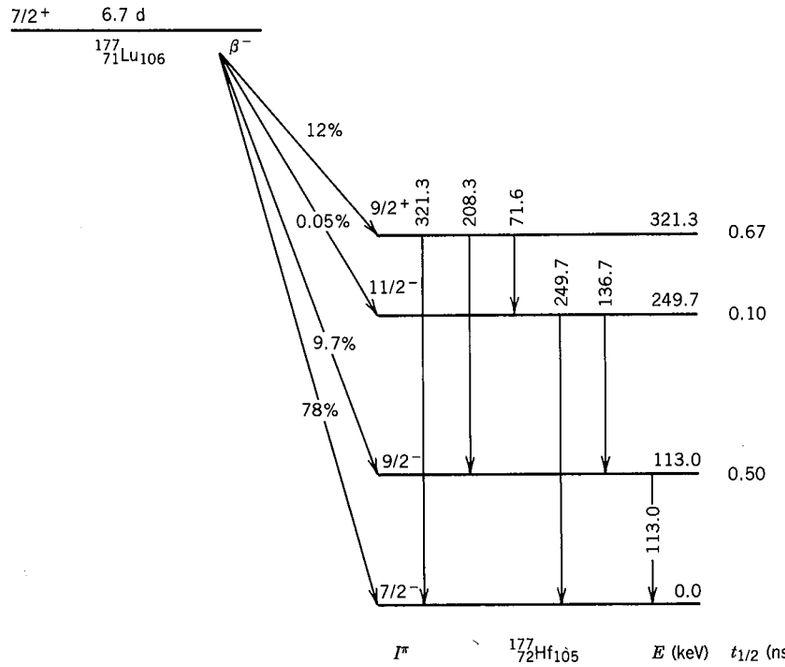

Figure 10.20 Decay scheme of ^{177}Lu to ^{177}Hf. The β branching intensities are deduced indirectly from the γ-ray intensities and differ from those of Figure 9.29.

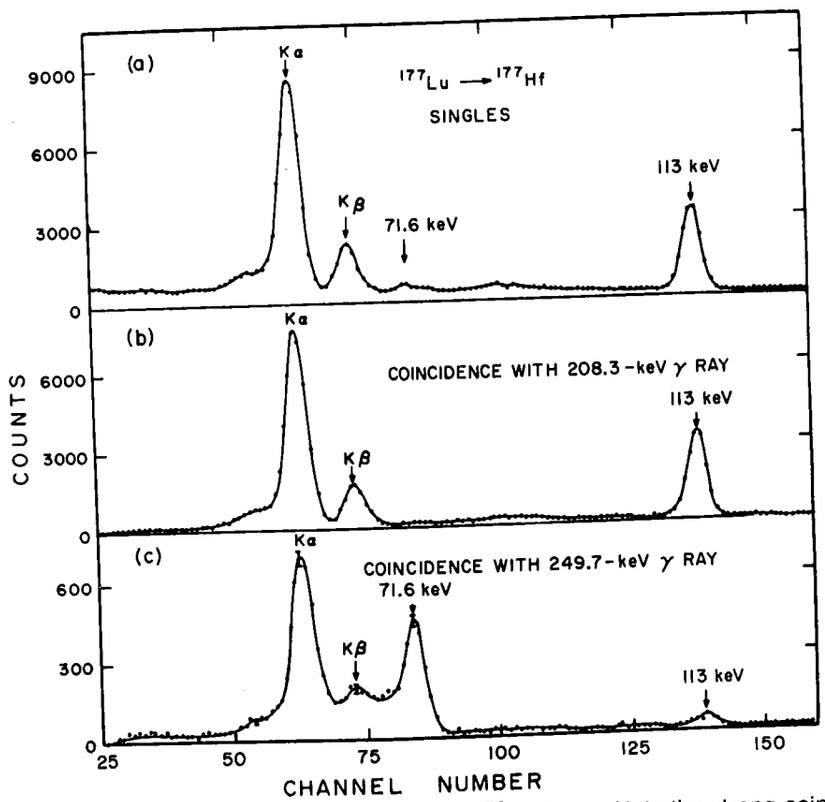

Figure 10.21 Coincidence spectra from the ^{177}Lu decay. Note the strong coincidence between 208 and 113; also note how the 71.6-keV peak, which is barely observable in the singles spectrum at the top, appears prominently in coincidence with 249.7 keV. (The small apparent 113.0-keV peak in the 249.7 keV coincidence spectrum is an artifact.) Data from A. P. Agnihotry et al., *Phys. Rev. C* **9**, 336 (1974).

The postulated decay scheme is shown in Figure 10.20. To verify our assumptions about the placement of the transitions, we can do γ-ray coincidence measurements, an example of which is shown in Figure 10.21. The coincidence spectrum shows quite plainly the 113.0–208.3 and 71.6–249.7 coincidence relationships.

As a final note on this decay, we point out that the L-subshell ratios can determine the relative $M1$ and $E2$ components of the 113.0-keV transition. Figure 10.22 shows the dependence of the L_I/L_{III} and L_I/L_{II} ratios on the $E2$ component. These very precise data show that the transition is 94–95% $E2$ and thus only 5–6% $M1$. In this case, the nuclear wave functions enhance the $E2$ transition probability to such an extent that $E2$ dominates over $M1$.

In this section we have given some examples of decay schemes that can be elucidated through γ-ray and conversion electron spectroscopy. It is of course impossible to isolate any one technique from all others in determining the properties of nuclear states, but from the examples discussed here you should

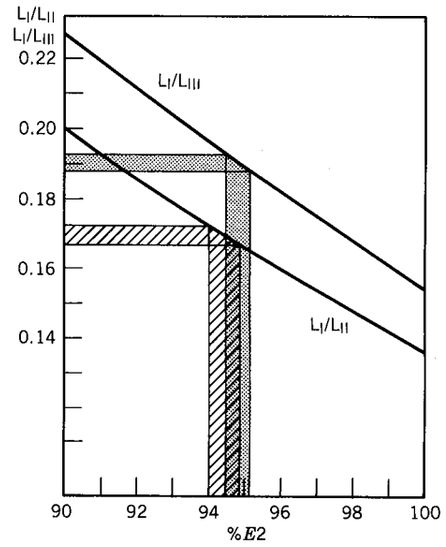

Figure 10.22 Determination of the $E2$ fraction of the 113.0-keV transition in ^{177}Hf from L-subshell data. The horizontal bars give the ranges of the experimental L-subshell ratios, and the vertical bars give the corresponding $E2$ fractions. The transition is deduced to be 94–95% $E2$ (and thus 5–6% $M1$). Data from S. Högberg et al., *Z. Phys.* **254**, 89 (1972).

appreciate the detailed and precise information that can be obtained from these methods.

10.9 NUCLEAR RESONANCE FLUORESCENCE AND THE MÖSSBAUER EFFECT

The inverse process of γ-ray emission is γ-ray absorption—a nucleus in its ground state absorbs a photon of energy E_γ and jumps to an excited state at an energy ΔE above the ground state. The relationship between E_γ and ΔE follows from a procedure similar to that used to obtain Equation 10.4:

$$\Delta E = E_\gamma - \frac{E_\gamma^2}{2Mc^2} \tag{10.28}$$

if we assume the absorbing nucleus to be initially at rest. The difference between ΔE and E_γ comes about because of the recoil of the nucleus after absorbing the photon.

Let us assume we have a source of γ radiation of continuously variable energy. The cross section for resonant absorption of a photon is

$$\sigma_0 = 2\pi\left(\frac{\hbar c}{E_\gamma}\right)^2 \frac{2I_e + 1}{2I_g + 1} \frac{1}{1 + \alpha} \tag{10.29}$$

where α is the total conversion coefficient and I_g and I_e are the spin quantum

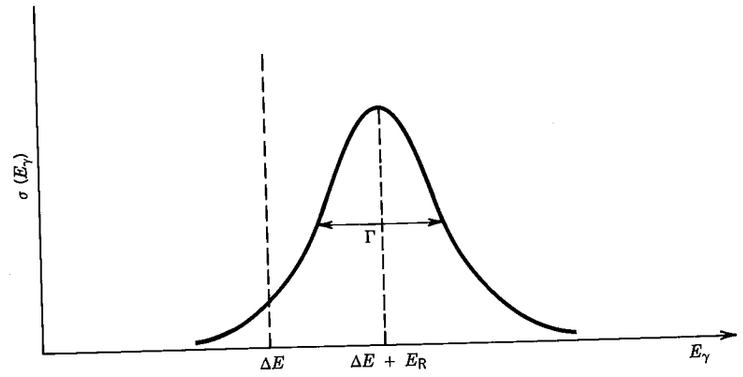

Figure 10.23 The resonant absorption cross section of Equation 10.30. The recoil energy E_R shifts the resonance slightly from the value $E_\gamma = \Delta E$ expected in the absence of recoil.

numbers of the ground and excited states. Because the energy of the excited state is not "sharp," the absorption will take place even when the γ energy differs somewhat from the resonant value. As we discussed in Chapter 6, any state that has a mean life τ has a width $\Gamma = \hbar/\tau$, and measurement of the energy of the state gives a distribution of the form of Equation 6.20 and Figure 6.3. If we were to pass a beam of photons through a collection of bare nuclei (so as to eliminate scattering and absorption processes due to atomic electrons), then the resonant absorption cross section is

$$\sigma(E_\gamma) = \sigma_0 \frac{(\Gamma/2)^2}{\left[E_\gamma - (\Delta E + E_R)\right]^2 + (\Gamma/2)^2} \tag{10.30}$$

where E_R is the recoil correction $E_\gamma^2/2Mc^2$. This distribution is plotted in Figure 10.23. For typical nuclear states of mean lives ns to ps, the widths will be in the range of 10^{-6} to 10^{-3} eV.

Figure 10.24 shows a schematic view of the resonant absorption experiment. As E_γ is varied, the resonance curve of Figure 10.23 is traced. At energies E_γ far

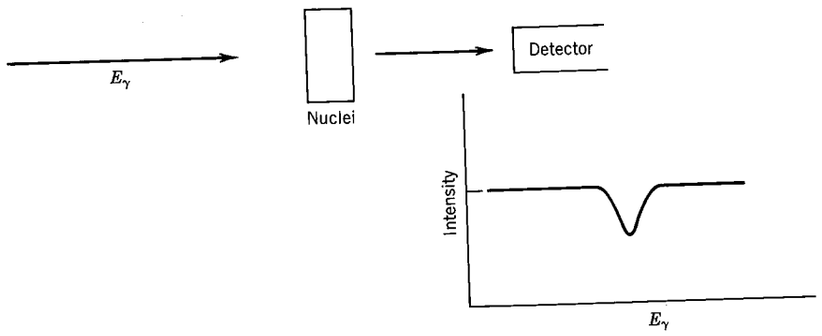

Figure 10.24 Schematic of an experiment to observe resonant absorption by nuclei.

from the resonance, the nuclei are transparent to the radiation, and no absorption occurs. At the resonance, the transmitted intensity reaches a minimum value.

In practice, we would be unlikely to observe the *natural linewidth* Γ. A primary additional contributor to the observed linewidth is the *Doppler broadening* Δ, which arises because the nuclei are not at rest (as we assumed) but in fact are in thermal motion at any temperature T. The photons as emitted or absorbed in the lab frame appear Doppler shifted with energies $E'_\gamma = E_\gamma(1 \pm v_x/c)$, where v_x is the velocity component along the photon direction. If the motion of the nuclei is represented by the usual Maxwell velocity distribution $e^{-[(1/2)mv_x^2]/kT}$ there will be a distribution of energies of the form $e^{-(mc^2/2kT)(1-E'_\gamma/E_\gamma)^2}$. This gives a Gaussian distribution of width

$$\Delta = 2\sqrt{\ln 2}\, E_\gamma \sqrt{\frac{2kT}{Mc^2}} \tag{10.31}$$

At room temperature, $kT \simeq 0.025$ eV, and for a 100-keV transition in a medium-weight nucleus $\Delta \simeq 0.1$ eV, which dominates the natural linewidth for most nuclear transitions. Even cooling to low temperature (for instance, to 4 K in thermal contact with a reservoir of liquid helium) reduces the width by only an order of magnitude to 0.01 eV. The width observed in experiments such as that of Figure 10.24 will be a combination of the natural linewidth plus additional contributions including Doppler broadening.

Tunable sources of photons of the sort needed for the resonance experiment do not exist. (The best one can do is the continuous electromagnetic spectrum from bremsstrahlung or synchrotron radiation produced by charged-particle accelerators capable of reaching relativistic energies.) In our laboratories, we must therefore make do with ordinary sources of γ radiation that emit only at discrete energies. However, to do the resonant absorption, we must find a radioactive source that emits a γ ray of an energy within at most 0.1 eV of the desired resonant energy $\Delta E + E_R$. It is of course extremely unlikely to find such radiation, and with the proper multipole character besides. It therefore makes sense for us to try to use a source in which the γ radiation is emitted in the same *downward* transition that we are trying to excite *upward* by resonant absorption. Consider, for example, the decay of ^{198}Au; following the β decay to ^{198}Hg, a single strong γ-ray of energy 412 keV is emitted. If we now allow that γ ray to fall upon a target of stable ^{198}Hg nuclei, there is a possibility of absorption and excitation from the ground state to the 412-keV excited state. The mean life of the 412-keV state is 32 ps, corresponding to a width of 2×10^{-5} eV. The recoil energy E_R is $E_\gamma^2/2Mc^2 = 0.46$ eV, and it is important to note that the recoil affects both the *emitted* and *absorbed* transitions. That is, the emitted radiation has energy $\Delta E - E_R$, while for absorption we must supply an energy of $\Delta E + E_R$. The situation is indicated in Figure 10.25, in which we have assumed the lines to have the room-temperature Doppler width of 0.36 eV. As you can see, there is minimal overlap between the emission and absorption lines, and thus little probability of resonant excitation.

(Contrast this with the case of atomic radiation. Optical transitions have energies of a few eV; the recoil correction in Hg would be 2.7×10^{-12} eV and there would be almost complete overlap between the profile of the source and

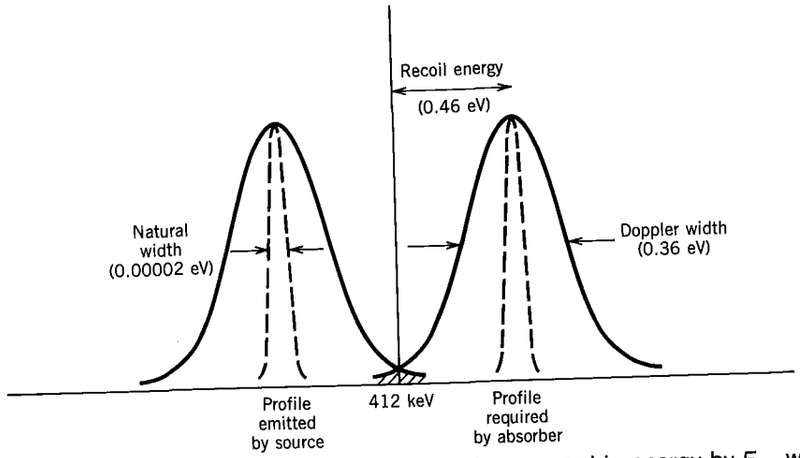

Figure 10.25 The emitted radiation is shifted downward in energy by E_R, while the absorption requires an energy shifted upward by E_R. Because of the Doppler (thermal) broadening, there is a small overlap (shaded region) between the emission and absorption lines. The natural width has been greatly exaggerated on the energy scale of the diagram.

absorber transitions. Atomic resonant absorption experiments are thus relatively easy to perform.)

There are several techniques for overcoming the energy difference $2E_R$ between the source and absorber transitions. The first consists of raising the temperature, thereby increasing the Doppler broadening and the overlap of the profiles. A second method is to move the source toward the absorber at high speed to Doppler shift the emitted energy by an amount $2E_R$. Since the Doppler-shifted energy is $E'_\gamma = E_\gamma(1 + v/c)$, the speed required is

$$v = c\frac{2E_R}{E_\gamma} \tag{10.32}$$

which gives $2.2 \times 10^{-6}c$, or 670 m/s. Experiments of this type are usually done by attaching the source to the tip of a rotor in a centrifuge spinning at 10^4–10^5 revolutions per minute. Figure 10.26 shows examples of results from the thermal-broadening and centrifuge techniques.

The most successful and useful technique for defeating the recoil problem is called the Mössbauer effect. In 1958, Rudolf Mössbauer performed a resonant absorption experiment using a source of ^{191}Ir (E_γ = 129 keV; E_R = 0.047 eV). The emitting and absorbing nuclei were bound in a crystal lattice. Typical binding energies of an atom in a lattice are 1–10 eV, and thus there is not enough recoil energy available for the atom to leave its lattice site. The effect is somewhat like the difference between hitting a single brick with a baseball bat and hitting one brick in a solid brick wall—the entire solid lattice absorbs the recoil momentum. The mass that appears in the expression for the recoil energy becomes the mass of the entire solid, rather than the mass of one atom. In addition, a certain fraction of the atoms in a lattice (determined from statistical considerations) is in the vibrational ground state of thermal motion and thus

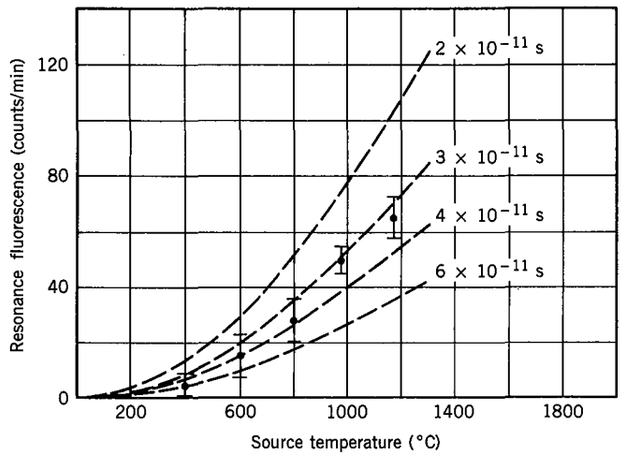

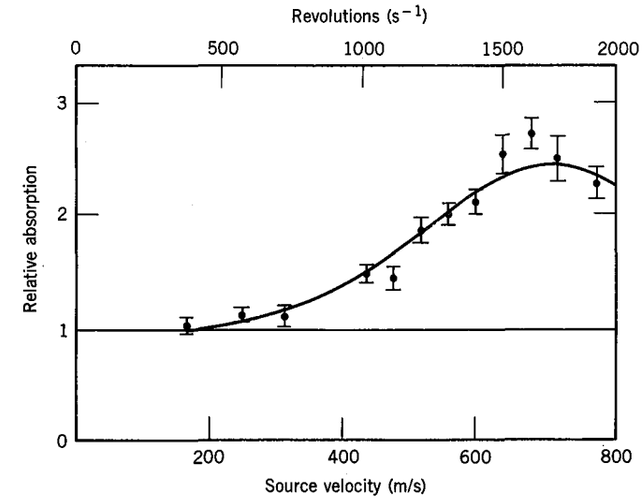

Figure 10.26 Thermal broadening (top) and centrifuge (bottom) techniques for observing nuclear resonance in ^{198}Hg. The data points at top show increasing resonant absorption as the temperature is increased (broadening the lines in Figure 10.25 and increasing the overlap). The dashed lines show the expected behavior for different excited-state lifetimes (that is, for different natural widths). From these data the lifetime is determined to be about 30 ps. The graph at bottom shows the result of Doppler shifting the radiation emitted by the source, by attaching it to the tip of a rotor. In this case, the emission line in Figure 10.25 is being moved to higher energy until it overlaps the absorption line. As estimated, this occurs at about 670 m/s. Thermal data from F. R. Metzger and W. B. Todd, *Phys. Rev.* **95**, 853 (1954); rotor data from W. G. Davey and P. B. Moon, *Proc. Phys. Soc. London A* **66**, 956 (1953).

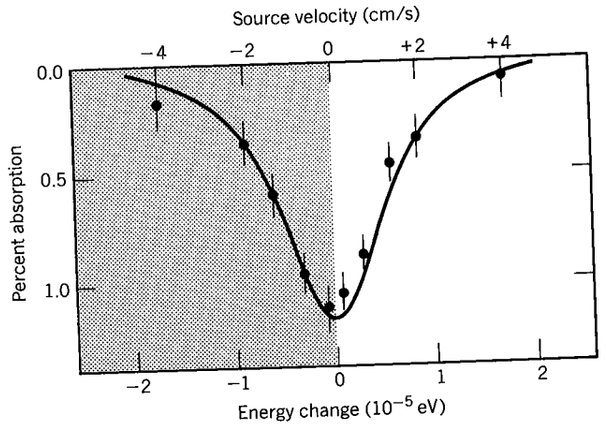

Figure 10.27 Mössbauer effect using 129-keV γ ray from ^{191}Ir. Because (1) the natural linewidth is obtained, and (2) the recoil is eliminated, there is essentially complete overlap between source and absorber. Doppler-shifting the source energy by an amount slightly greater that the natural linewidth (10^{-5} eV) is sufficient to destroy the resonance. From original data by R. Mössbauer, *Z. Naturforsch. A* **14**, 211 (1959).

shows very little thermal Doppler broadening. The result is very narrow and overlapping emission and absorption lines, each characterized by the natural linewidth (3×10^{-6} eV in ^{191}Ir). To demonstrate this phenomenon, we have only to move the source and absorber relative to one another at low speed; if the speed is such that the Doppler shift is greater than the natural linewidth, the resonance will be destroyed. For a total linewidth of 6×10^{-6} eV (because both source and absorber have the natural width), the necessary speed is about $5 \times 10^{-11}c$, or about 15 mm/s, a considerable improvement over the 700 m/s needed for the centrifuge experiment! Figure 10.27 shows the resulting resonance, first obtained by Mössbauer in 1958.

What is remarkable about the Mössbauer effect is its extreme precision for the measurement of relative energies. For instance, suppose we modified the environment of the source or absorber nuclei in such a way that the energy difference between the initial and final nuclear states shifted by a very small amount δE. Using the Mössbauer effect, we should be able to measure this shift, as long is it is of the same order as the width of the resonance. (If the shift is too small compared with the width of the resonance, it is very difficult to measure.) In the case of ^{191}Ir, where the observed width is about 10^{-5} eV, this would amount to measuring a change in energy of 10^{-5} eV out of a gamma-ray energy of 10^5 eV, or an effect of one part in 10^{10}. In ^{57}Fe, which is more frequently used for the Mössbauer effect, the observed (natural) linewidth is of order 10^{-8} eV, and in this case experimental effects of the order of one part in 10^{12} can be measured!

Although we will not go into the details of the theory of the Mössbauer effect, it is worthwhile to consider briefly one other aspect of the resonance, its depth, which is determined by the fraction of the nuclei in the lattice that emits (or absorbs) with no recoil. The calculation of the recoil-free fraction f depends on properties of the solid more detailed than the simple question of whether or not

the recoil energy exceeds the lattice binding energy. Solids can absorb energy in many ways other than by removing atoms from their lattice sites. At low energies and temperatures, the primary way is through lattice vibrations, called *phonons*. (Propagation of these phonons through a lattice is responsible for familiar properties such as mechanical and acoustical waves.) These vibrations occur at a spectrum of frequencies, from zero up to a maximum, ω_{max}. The energy corresponding to the highest vibrational frequency is usually expressed in terms of the corresponding temperature, called the *Debye temperature*, θ_D, defined so that $\hbar\omega_{max} = k\theta_D$, where k is the Boltzmann constant. For typical materials, $\hbar\omega_{max} \sim 0.01$ eV and $\theta_D \sim 1000$ K. The recoilless fraction is

$$f = \exp\left[-\frac{\langle x^2\rangle}{(\lambda/2\pi)^2}\right] \tag{10.33}$$

where $\langle x^2\rangle$ is the mean-square vibrational amplitude of the emitting nucleus and λ is the wavelength of the γ ray. Using the Bose-Einstein distribution function for the vibrational phonon spectrum permits the calculation of the mean-square amplitude, and gives for the recoilless fraction

$$f = \exp\left\{-\frac{6E_R}{k\theta_D}\left[\frac{1}{4} + \left(\frac{T}{\theta_D}\right)^2 \int_0^{\theta_D/T} \frac{x\,dx}{e^x - 1}\right]\right\} \tag{10.34}$$

At low temperatures $T \ll \theta_D$, the last term in the exponent is negligible. Values of θ_D do not vary greatly among metals ($\theta_D \sim 400$ K for Fe and 300 K for Ir), so the recoil energy E_R is essential in determining the recoilless fraction. For the 14.4 keV transition of ^{57}Fe, $E_R = 0.002$ eV and $f = 0.92$, while for Ir, $f \approx 0.1$. (The second term in the exponent of Equation 10.34 is always negative, and thus this term will work to make f smaller than these low-temperature estimates.) Because recoilless processes are needed in both the source and absorber, the overall recoilless fraction is determined by the product of the factors in the source and absorber. It is therefore not surprising that Mössbauer's original experiment with Ir showed an effect of only 1%, while Fe shows a much larger effect.

The Mössbauer effect has found applications in an enormous variety of areas. Its primary usefulness is in those applications in which we must determine the properties of the physical or chemical environment of a nucleus, but an important exploitation of the extreme precision of the method was the determination of the change in energy of photons falling in the gravitational field of the Earth, called the *gravitational red shift*. One of the cornerstones of Einstein's General Theory of Relativity is the Principle of Equivalence, according to which the effects of a local uniform gravitational field cannot be distinguished from those of a uniformly accelerated reference frame. If we were to observe the emission and absorption of radiation in an accelerated reference frame, in which H is the distance between the source and absorber, then in the time H/c necessary for radiation to travel from the source to the absorber, the absorber would acquire a velocity gH/c, where g is the acceleration, chosen to be numerically equal (and in the opposite direction) to the gravitational acceleration of the uniform field. The radiation photons are therefore Doppler shifted,

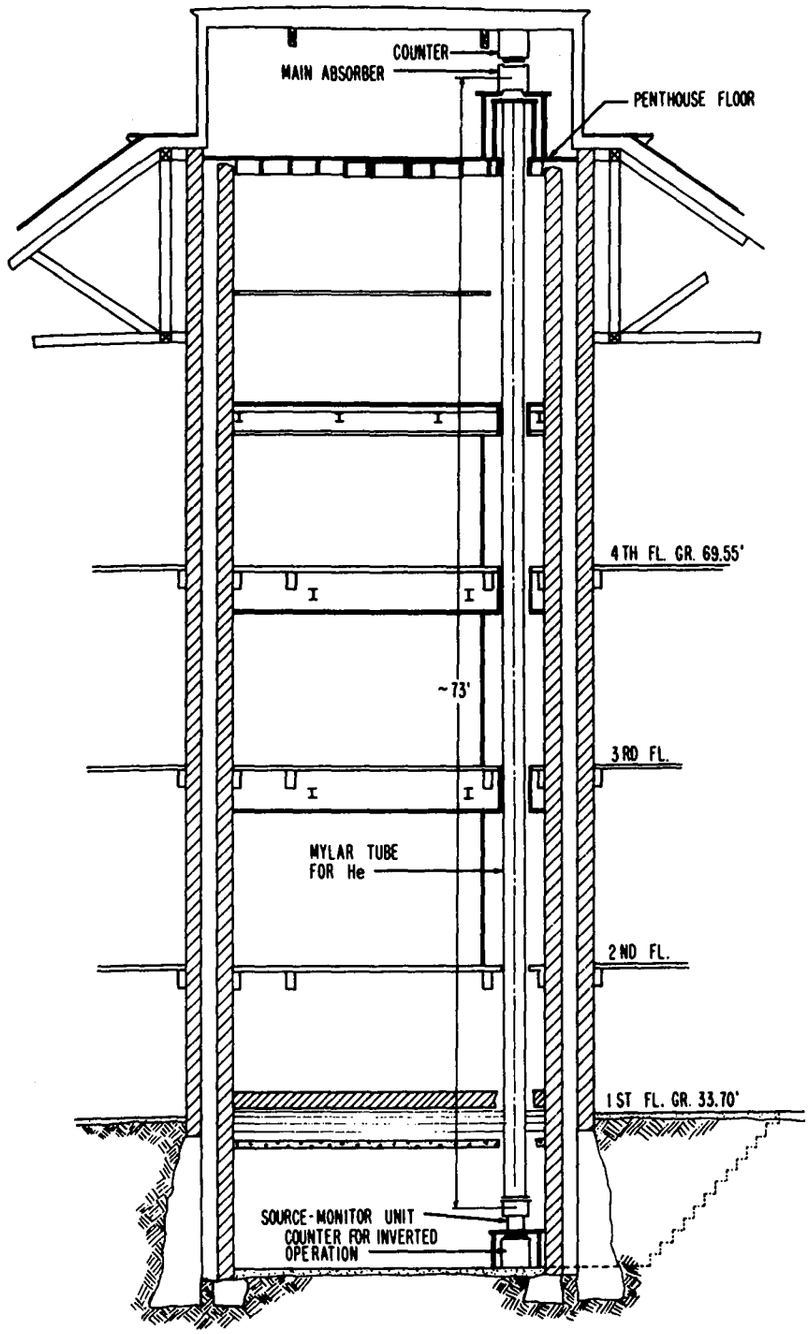

Figure 10.28 Schematic view of the gravitational red shift experiment in the Harvard tower. To reduce absorption in air, the 14.4-keV photons traveled in He gas in a Mylar tube. In the configuration shown, the source is at the bottom and the absorber and counter are at the top. From R. V. Pound, in *Mössbauer Spectroscopy II*, edited by U. Gonser (Berlin: Springer-Verlag, 1981), p. 31.

according to

$$\frac{\Delta E}{E} = \frac{\Delta v}{c} = \frac{gH}{c^2} \tag{10.35}$$

This amounts to about 1×10^{-16} per meter in the Earth's gravitational field.

In the original experiment of Pound and Rebka, *Phys. Rev. Lett.* **4**, 337 (1960), ^{57}Fe was used (from a 1-Ci source of ^{57}Co), and the 14.4-keV photons were allowed to travel 22.5 m up the tower of the Jefferson Physical Laboratory at Harvard (Figure 10.28). The expected effect was of order 2×10^{-15}, which required heroic efforts even for ^{57}Fe with a sensitivity (Γ/E_γ) of roughly 3×10^{-13}. To observe the small shift (about 10^{-2} of the width of the resonance), Pound and Rebka concentrated on the portions of the sides of the resonance curve with the largest slope. To reduce systematic effects, it was necessary to monitor with great precision the temperature of the source and absorber (temperature differences between source and absorber would cause unequal Doppler broadenings, which would simulate a shift in the peak) and periodically to interchange source and absorber to allow the photons to travel in the opposite direction. After four months of experiments, the result was $\Delta E/E = (4.902 \pm 0.041) \times 10^{-15}$, compared with the expected value 4.905×10^{-15} for the 45-m round trip. This careful experiment represents one of the most precise tests of the General Theory of Relativity, and it would not have been possible without the great sensitivity provided by the Mössbauer effect. [For a review of this experiment, see R. V. Pound, in *Mössbauer Spectroscopy II*, edited by U. Gonser (Berlin: Springer-Verlag, 1981), p. 31.]

As mentioned above, perhaps the primary application of the Mössbauer effect has been in studying the interaction of nuclei with their physical and chemical environments. The interaction of nuclear electromagnetic moments with the fields

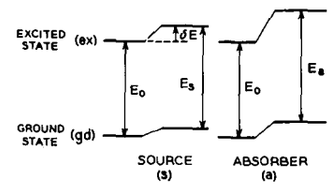

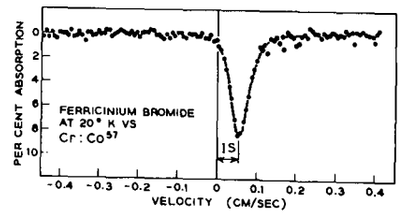

Figure 10.29 The isomer shift. In different materials, the ground and excited states show different shifts from the overlap of electronic wave functions with the nucleus. The effect on the resonance is to shift it away from zero relative velocity. From G. K. Wertheim, *Mössbauer Effect: Principles and Applications* (New York: Academic, 1964).

of the environment is usually called *hyperfine interactions*, and will be discussed in more detail in Chapter 16. For the present, we give a few examples of the application of Mössbauer spectroscopy to their study.

In the first case, we measure simply the effect of the penetration of atomic wave functions into the nuclear volume. This quantity, called ΔE in Equation 3.12, represents the difference in energy between electronic levels calculated for a "point" nucleus and for a uniformly charged spherical nucleus of radius R. Although our goal in Chapter 3 was to calculate the effect on the atomic levels, a bit of thought should convince you that nuclear levels should be shifted by an equal but opposite energy because the observed total (atomic + nuclear) energy cannot change under the influence of internal forces. If we let E_0 represent the photon energy in the absence of this effect ($E_0 = E_e - E_g$, where e is the excited state and g is the ground state), then the observed energy is

$$\begin{aligned} E &= (E_e + \Delta E_e) - (E_g + \Delta E_g) \\ &= E_0 + \Delta E_e - \Delta E_g \end{aligned} \tag{10.36}$$

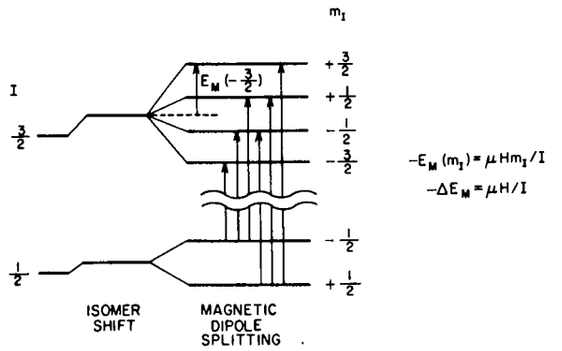

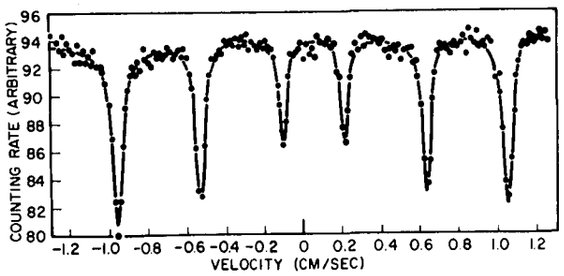

Figure 10.30 Magnetic dipole splitting of nuclear levels observed with the Mössbauer effect. At top right are shown the nuclear m states split by a magnetic field. If the ground state and excited state have different nuclear magnetic dipole moments, the energy splittings ΔE_M will be different, as shown; in the case illustrated, the moments also have opposite signs. For dipole transitions, only $\Delta m_I = 0$ or ± 1 can occur, so 6 individual components are seen. From G. K. Wertheim, *Mössbauer Effect: Principles and Applications* (New York: Academic, 1964).

because the ground and excited states will have different nuclear wave functions and thus different radii. If the source and absorber in a Mössbauer experiment had the same chemical environment, the resonance would not be affected, but if the source and absorber are different, then the transition energies are slightly different. In this case, one of the peaks in Figure 10.25 would be shifted somewhat, relative to where it appears when the source and absorber are similar. The effect on the Mössbauer spectrum is to shift the center of the resonance away from zero velocity. This effect is called the *isomer shift* (or sometimes *chemical shift*) and is illustrated in Figure 10.29. You can see that this is a small effect, of the order of one part in 10^{12}.

In another kind of hyperfine coupling, we study the splitting of the nuclear levels in a magnetic field. In atomic physics, the effect of a magnetic field on spectral lines is called the *Zeeman effect* and corresponds to the removal of the m degeneracy of a level of angular momentum I in a magnetic field—the field splits the level into $2I + 1$ equally spaced sublevels. Atomic wavelengths are typically shifted by one part in 10^4 by the Zeeman effect; nuclear magnetic moments are only 10^{-3} of atomic magnetic moments, and nuclear transition energies are 10^5 of atomic energies, and so the resulting nuclear effect is one part in 10^{12}. Figure

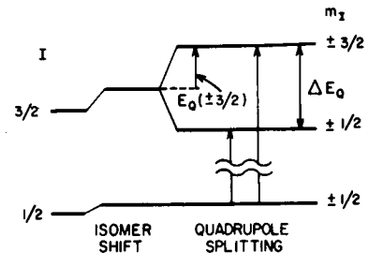

$$E_Q(m_I) = eqQ\left[\frac{3m_I^2 - I(I+1)}{4I(2I-1)}\right]$$

$$\Delta E_Q = E_Q(3/2) - E_Q(1/2) = \frac{eqQ}{2}$$

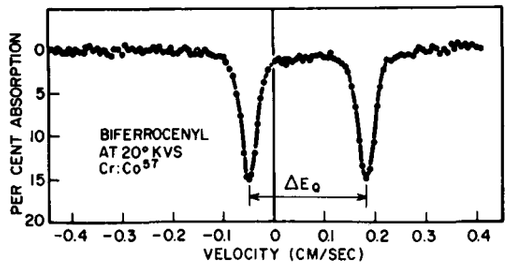

Figure 10.31 Electric quadrupole hyperfine splitting. In the expression for the splitting energy, Q represents the nuclear electric quadrupole moment and q is the electric field gradient (sometimes called V_{zz} or $\partial^2 V / \partial z^2$). In this case only two lines appear; in addition there is an isomer shift that moves the center of the Mössbauer spectrum away from zero velocity. From G. K. Wertheim, *Mössbauer Effect: Principles and Applications* (New York: Academic, 1964).

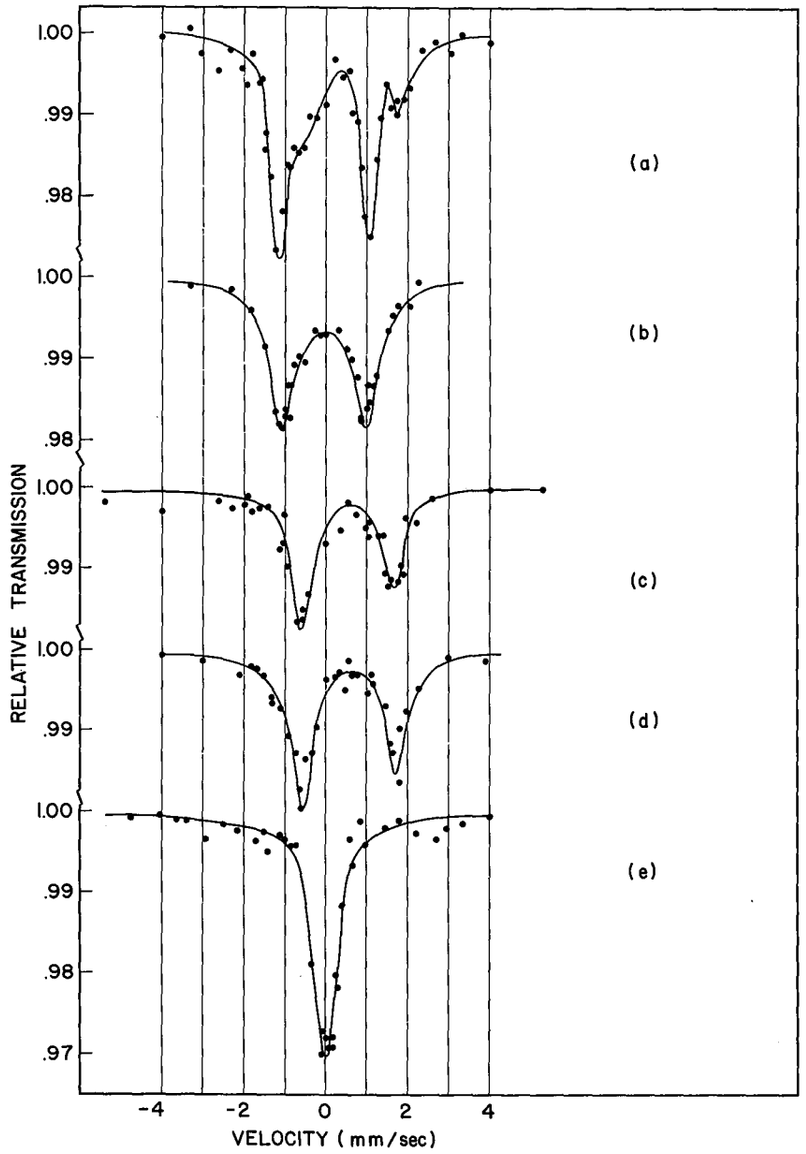

Figure 10.32 Mössbauer effect experiments showing the differing chemical environments of Fe in hemoglobin. The source for these experiments was ^{57}Co (which decays to ^{57}Fe) in Pt; absorbers were (*a*) rat red cells at 4 K, (*b*) oxygenated rat hemoglobin at 77 K, (*c*) human hemoglobin in CO_2 at 77 K, (*d*) human hemoglobin in N_2 at 77 K, and (*e*) human hemoglobin in CO at 77 K. Note the different isomer shifts and electric quadrupole splittings. From U. Gonser et al., *Science* **143**, 680 (1964). Copyright © 1964, AAAS.

10.30 shows an example of this for ^{57}Fe. An isomer shift is present, in addition to the magnetic hyperfine structure. The magnetic moments of the ground and excited states are unequal, and in fact the Mössbauer spectrum can give the magnetic moment of the excited state to great precision, when (as in ^{57}Fe) the ground state is stable and its moment is precisely known. It is also possible, if the moment is known, to deduce the size of the magnetic field, the determination of which can give important clues about atomic structure.

Finally, the nuclear quadrupole moment can interact with an electric field gradient to give an electric quadrupole splitting. This splitting is proportional to m^2 and thus does not distinguish between $+m$ and $-m$. Furthermore, it vanishes when $I = \frac{1}{2}$. Figure 10.31 shows an example in the case of ^{57}Fe. Note that 2 lines appear in the case of electric quadrupole interactions in ^{57}Fe (whereas 6 appear in the magnetic dipole case). For other isotopes having different ground-state and excited-state spins, the number of lines will be different.

These same studies can be extended to materials with a variety of applications. For example, the protein hemoglobin gives blood its red color and is responsible for binding to the oxygen in the bloodstream. Hemoglobin is rich in Fe and can therefore be used in Mössbauer experiments. Figure 10.32 shows some typical results. Oxygenated blood shows a quadrupole-split Mössbauer spectrum, but with an isomer shift slightly different from that of deoxygenated blood. Venous blood shows a mixture of the two types. Blood exposed to CO shows neither quadrupole splitting nor isomer shift. Oxygenated hemoglobin shows magnetic dipole splittings when placed in a strong magnetic field; deoxygenated hemoglobin does not. All of the above refer to the ferrous ion (Fe^{2+}); ferric ions (Fe^{3+}), the presence of which may indicate certain blood diseases, give very different Mössbauer spectra.

REFERENCES FOR ADDITIONAL READING

A comprehensive work on electromagnetic multipole radiation is M. E. Rose, *Multipole Fields* (New York: Wiley, 1955); Chapter 12 of J. M. Blatt and V. F. Weisskopf, *Theoretical Nuclear Physics* (New York: Wiley, 1952) also discusses classical multipole radiation. The quantum mechanics of the electromagnetic radiation field is considered in detail in Sections 3.1–3.9 of M. G. Bowler, *Nuclear Physics* (Oxford: Pergamon, 1973). Also of interest are Chapters 15 (multipole radiation) and 16 (internal conversion) of *Alpha-, Beta- and Gamma-Ray Spectroscopy*, edited by K. Siegbahn (Amsterdam: North-Holland, 1965).

Many theoretical and experimental aspects of γ emission are reviewed in *The Electromagnetic Interaction in Nuclear Spectroscopy*, edited by W. D. Hamilton (Amsterdam: North-Holland, 1975).

Tabulations of theoretical conversion coefficients can be found in R. S. Hager and E. C. Seltzer, *Nuclear Data Tables A* **4**, 1 (1968); F. Rösel, H. M. Fries, K. Alder, and H. C. Pauli, *Atomic Data and Nuclear Data Tables* **21**, 91 (1978); L. A. Sliv and I. M. Band, in *Alpha-, Beta- and Gamma-Ray Spectroscopy*, edited by K. Siegbahn (Amsterdam: North-Holland, 1965), Appendix 5.

The Mössbauer effect is reviewed in G. K. Weitheim, *Mössbauer Effect: Principles and Applications* (New York: Academic, 1964), and T. C. Gibb,

Principles of Mössbauer Spectroscopy (New York: Halsted, 1976). Collections of recent papers on the application of the Mössbauer effect are *Applications of Mössbauer Spectroscopy*, Vols. I and II, edited by Richard L. Cohen (New York: Academic, 1976 and 1980), and *Mössbauer Spectroscopy*, edited by U. Gonser (Berlin: Springer-Verlag, 1981).

PROBLEMS

1. Each of the following nuclei emits a photon in a γ transition between an excited state and the ground state. Given the energy of the photon, find the energy of the excited state and comment on the relationship between the nuclear recoil energy and the experimental uncertainty in the photon energy: (a) 320.08419 ± 0.00042 keV in ^{51}V; (b) 1475.786 ± 0.005 keV in ^{110}Cd; (c) 1274.545 ± 0.017 keV in ^{22}Ne; (d) 3451.152 ± 0.047 keV in ^{56}Fe; (e) 884.54174 ± 0.00074 keV in ^{192}Ir.

2. Following the decay of ^{198}Au, three γ's are observed to be emitted from states in ^{198}Hg; their energies (in keV) are γ_1, 411.80441 ± 0.00015; γ_2, 675.88743 ± 0.00069; and γ_3, 1087.69033 ± 0.00074. It is suggested that there are two excited states E_1 and E_2 in ^{198}Hg that are populated in the decay, and that the γ's correspond respectively to the transitions $E_1 \rightarrow E_0$, $E_2 \rightarrow E_1$, and $E_2 \rightarrow E_0$ (where E_0 represents the ground state). If this hypothesis were correct, we would expect $E_{\gamma_1} + E_{\gamma_2} = E_{\gamma_3}$, which is almost but not quite true according to the experimental uncertainties. Show how the proper inclusion of the nuclear recoil resolves the discrepancy.

3. The calculation of the emission probability for electric quadrupole radiation involves a term of the form of Equation 3.36, with the proper labeling of initial and final wave functions. From such an integral, verify the parity selection rule for electric quadrupole transitions.

4. (a) For a light nucleus ($A \approx 10$), compute the ratio of the emission probabilities for quadrupole and dipole radiation according to the Weisskopf estimates. Consider all possible choices for the parities of the initial and final states. (b) Repeat for a heavy nucleus ($A \approx 200$).

5. In a nucleus described by the rotational model (see Figure 5.22), the second excited state is always 4^+. This state decays by $E2$ radiation to the 2^+ state. Justify this observation by calculating, using the Weisskopf estimates, the ratio between the $E2$ decay probability and (a) the octupole ($L = 3$) and hexadecapole ($L = 4$) decays to the 2^+ state and (b) the hexadecapole decay to the ground state. (*Note*: These are collective rotational states, for which the Weisskopf estimates should not be taken too seriously.)

6. For the following γ transitions, give all permitted multipoles and indicate which multipole might be the most intense in the emitted radiation.

(a) $\frac{9}{2}^- \rightarrow \frac{7}{2}^+$ (d) $4^+ \rightarrow 2^+$
(b) $\frac{1}{2}^- \rightarrow \frac{7}{2}^-$ (e) $\frac{11}{2}^- \rightarrow \frac{3}{2}^+$
(c) $1^- \rightarrow 2^+$ (f) $3^+ \rightarrow 3^+$

7. A certain decay process leads to final states in an even-Z, even-N nucleus and gives only three γ rays of energies 100, 200, and 300 keV, which are found to be (respectively) of $E1$, $E2$, and $E3$ multipolarity. Construct two different possible level schemes for this nucleus (consistent with known systematics of nuclear structure) and label the states with their most likely spin-parity assignments. Suggest experiments that might distinguish between your proposed level schemes.

8. A nucleus has the following sequence of states beginning with the ground state: $\frac{3}{2}^+$, $\frac{7}{2}^+$, $\frac{5}{2}^+$, $\frac{1}{2}^-$, and $\frac{3}{2}^-$. Draw a level scheme showing the intense γ transitions likely to be emitted and indicate their multipole assignment.

9. The isomeric 2^+ state of ^{60}Co at 58.6 keV decays to the 5^+ ground state. Internal conversion competes with γ emission; the observed internal conversion coefficients are $\alpha_K = 41$, $\alpha_L = 7$, $\alpha_M = 1$. (a) Compute the expected half-life of the 2^+ state if the transition multipolarity is assumed to be $M3$, and compare with the observed half-life of 10.5 min. (b) If the transition also contained a small component of $E4$ radiation, how would your estimate for the half-life be affected? (c) The 2^+ state also decays by direct β emission to ^{60}Ni. The maximum β energy is 1.55 MeV and the log ft is 7.2. The 2^+ state decays 0.25% by β emission and 99.75% by γ emission and internal conversion. What is the effect on the calculated half-life of including the β emission?

10. An even-Z, even-N nucleus has the following sequence of levels above its 0^+ ground state: 2^+ (89 keV), 4^+ (288 keV), 6^+ (585 keV), 0^+ (1050 keV), 2^+ (1129 keV). (a) Draw an energy level diagram and show all reasonably probable γ transitions and their dominant multipole assignments. (b) By considering also internal conversion, what additional transitions and multipoles would appear?

11. (a) Pick half a dozen or so typical examples of $2^+ \rightarrow 0^+$ transitions from the first excited states of "rotational" nuclei, $150 < A < 190$. (Use standard reference works for nuclear spectroscopic data.) Compute the ratio between the observed γ decay rate and the corresponding Weisskopf estimate. Be sure to correct the measured lifetimes for internal conversion if necessary. (b) Repeat for "vibrational" nuclei, $60 < A < 150$, excluding cases at closed shells. (c) Draw any apparent conclusion about the difference between "rotational" and "vibrational" γ transitions.

12. The *Table of Isotopes* shows multipole assignments of γ transitions and lifetimes of excited states. By searching through the data given there, prepare a graph similar to Figure 10.13 showing the lifetimes for $M2$ transitions. Verify the dependence on the transition energy. (Be sure to use the *partial* lifetime in the cases in which a level can decay through several transitions.) Among the cases you should consider are ^{39}Ar, ^{73}As, ^{147}Eu, ^{165}Ho, ^{181}Ta, and ^{182}W, but you should find many other instances as well.

13. Among the nuclei in which there are known $E4$ transitions are ^{44}Sc, ^{52}Mn, ^{86}Rb, ^{93}Mo, ^{114}In, and ^{202}Pb. Look up the partial lifetimes for these transitions from collections of spectroscopic data, and compare with values calculated from the Weisskopf estimates.

14. The isotope ^{113}Cd captures a very low-energy neutron, leading to an excited state of ^{114}Cd, which emits a γ ray leading directly to the ^{114}Cd ground

state. (a) Find the energy of the γ ray, neglecting the nuclear recoil. (b) Calculate the kinetic energy of the recoiling ^{114}Cd.

15. In Section 5.2, the states of the vibrational model for even-Z, even-N nuclei up to the 0^+, 2^+, 3^+, 4^+, 6^+ three-phonon multiplet were discussed. The model also gives selection rules for γ emission: the phonon number must change by exactly one unit, and only $E2$ transitions are permitted. Draw a vibrational level scheme showing all permitted γ transitions starting with the three-phonon multiplet (use Figure 5.19 as a basis).

16. A certain decay scheme shows the following γ energies (in keV): 32.7, 42.1, 74.8, 84.0, 126.1, and 158.8. Coincidence studies reveal two features of the decay: only one of the γ's has none of the others in coincidence with it, and none of the γ's is in coincidence with more than three of the others. The γ's are preceded by a β decay that populates only one level. From this information suggest a possible level scheme. (*Note*: There are two different arrangements of the γ's that are consistent with the information given.)

17. In a study of the conversion electrons emitted in a decay process, the following electron energies were measured (in keV): 207.40, 204.64, 193.36, 157.57, 154.81, 143.53, 125.10, 75.27, 49.03, 46.27, 34.99. The electron binding energies are known to be 83.10 keV (K shell), 14.84 keV (L shell), 3.56 keV (M shell), and 0.80 keV (N shell). What is the minimum number of γ's that can produce the observed electron groups, and what are the γ energies?

18. Based on the information given in Figure 10.18 and Table 10.2, find all partial lifetimes for γ and electron emission for the 8^- level of ^{180}Hf.

19. For each of the following Mössbauer-effect transitions compute the natural width, the Doppler width at room temperature, the Doppler width at liquid helium temperature (4 K), and the nuclear recoil energy: (a) 73 keV, 6.3 ns in ^{193}Ir; (b) 14.4 keV, 98 ns in ^{57}Fe; (c) 6.2 keV, 6.8 μs in ^{181}Ta; (d) 23.9 keV, 17.8 ns in ^{119}Sn; (e) 95 keV, 22 ps in ^{165}Ho. Half-lives are given.

20. The absorption of the 27.8 keV magnetic dipole Mössbauer transition in ^{129}I takes the nucleus from its $\frac{7}{2}^+$ ground state to a $\frac{5}{2}^+$ excited state. The values of the magnetic dipole and electric quadrupole moments are: $\mu(\frac{7}{2}) = +2.6\ \mu_N$, $\mu(\frac{5}{2}) = +2.8\ \mu_N$, $Q(\frac{7}{2}) = -0.55$ b, $Q(\frac{5}{2}) = -0.68$ b. Make a sketch of the m-state splittings (similar to Figures 10.30 and 10.31) for the magnetic dipole and electric quadrupole cases and show the number of components in the Mössbauer spectrum. *Hint*: The magnetic field (B or H) and the electric field gradient (q or V_{zz}) can be regarded as positive.

21. In most of our work in nuclear physics, we regard the decay constant λ as a true constant for a given nuclear species. However, in this chapter and in the previous chapter you have studied two processes in which the nuclear decay rate could be sensitive to the chemical state of the atom. Discuss these two processes and explain how the atomic state might influence the nuclear decay rate. [For a discussion and some examples of cases in which this can occur, see the review by G. T. Emery, *Ann. Rev. Nucl. Sci.* **22**, 165 (1972).]

UNIT III
NUCLEAR REACTIONS